理學博士學位請求論文

A Strategy of *Vibrio vulnificus* to Turn off Flagellar Motility in the Presence of Glucose

패혈증 비브리오균에서 포도당 유무에 따른 운동성 조절

2018년 2월

서울大學校 大學院

生物物理 및 化學生物學科

朴 昭 暎

A Strategy of *Vibrio vulnificus* to Turn off Flagellar Motility in the Presence of Glucose

by

Soyoung Park

Under the supervision of

Professor Yeong-Jae Seok, Ph. D

A Thesis for the Degree of **Doctor of Philosophy**

February, 2018

Department of Biophysics and Chemical Biology

Seoul National University

패혈증 비브리오균에서 포도당 유무에 따른 운동성 조절

指導敎授 石 暎 宰

이 論文을 理學博士 學位論文으로 提出함

2017年 12月

서울大學校 大學院

生物物理 및 化學生物學科

朴 昭 暎

朴昭暎의 理學博士學位論文을 認准함

2017年 12月

委 員 長 _____

副委員長 _____

委 員 _____

委 員 _____

委 員 _____

ABSTRACT

A Strategy of *Vibrio vulnificus* to Turn off Flagellar Motility in the Presence of Glucose

Soyoung Park
Department of Biophysics and Chemical Biology
The Graduate School
Seoul National University

To survive in a continuously changing environment, bacteria sense concentration gradients of attractants or repellents, and purposefully migrate until a more favourable habitat is encountered. While glucose is known as the most effective attractant, the flagellar biosynthesis and hence chemotactic motility has been known to be repressed by glucose in some bacteria. To date, the only known regulatory mechanism of the repression of flagellar synthesis by glucose is via downregulation of the cAMP level, as shown in a few members of the family *Enterobacteriaceae*. In this thesis, it has been shown in *Vibrio vulnificus*, motile and curved rod-shaped halophilic bacterium with a single polar flagellum, the glucose mediated inhibition of flagellar motility operates by a completely different mechanism. In the presence of glucose, glucose-specific enzyme IIA ($EIIA^{Glc}$) of the phosphoenolpyruvate: sugar phosphotransferase system is dephosphorylated and inhibits the polar localization of FapA (flagellar assembly protein A) by sequestering it from the flagellated pole. A loss or delocalization of

FapA results in a complete failure of flagellation and motility. However, when glucose is depleted, $EIIA^{Glc}$ is phosphorylated and releases FapA such that free FapA can be localized back to the pole and trigger flagellation. The ligand fishing experiment revealed that FapA interacts with not only $EIIA^{Glc}$ but also a polar landmark protein, HubP (hub of the pole), which anchors client proteins to the cell poles and modulates the localization of the chromosome origin, chemotactic signaling proteins and flagellum. In the absence of HubP, FapA is diffused throughout the cytoplasm, indicating that proper polar targeting of FapA depends on HubP. HubP competes with dephosphorylated $EIIA^{Glc}$ for binding to FapA to regulate the early stage of flagellar assembly. Together, these results suggest that dephosphorylated $EIIA^{Glc}$ inhibits flagellation by sequestrating FapA from polar localized HubP in the presence of glucose and thereby enables *V. vulnificus* cells to adapt to and stay in a glucose-rich environment.

Key words:
flagellar motility; glucose signaling; protein localization; protein-protein interaction; PTS

***Student Number*: 2012-31269**

Contents

List of Figures

List of Tables

ABBREVIATIONS

PTS, phosphoenolpyruvate: carbohydrate phosphotransferase system

PEP, phosphoenolpyruvate

EI, enzyme I of the PTS

HPr, histidine-containing phosphocarrier protein

$EIIA^{Glc}$, glucose specific enzyme IIA of the PTS

CCR, carbon catabolite repression

cAMP, cyclic AMP; 3',5'-cyclic adenosine monophosphate

AC, adenylate cyclase

Glc, glucose

Mtl, mannitol

Gal, galactose

Gly, glycerol

HBB, hook basal body

MCP, methyl-accepting chemotaxis proteins

vIDE, *Vibrio* insulin degrading enzyme

FapA, flagellar assembly protein A

HubP, hub of the pole

MALDI-TOF, matrix-associated laser desorption ionization time-of-flight

SDS, sodium dodecyl sulfate

PAGE, polyacrylamide gel electrophoresis

DDM, *n*-dodecyl-β-D-maltoside

SPR, sulface plasmon resonance

GFP, green fluorescent protein

RFP, red fluorescent protein

PBS, phosphate-buffered saline

qRT-PCR, quantitative real-time polymerase chain reaction

RT-PCR, reverse transcription polymerase chain reaction

5’ RACE, 5’ rapid amplification of cDNA ends

Chapter I. Introduction

1. Background information on *Vibrio vulnificus*

1.1. Overview of *V. vulnificus*

Vibrio vulnificus is a Gram-negative, motile and curved rod-shaped halophilic bacterium with a single polar flagellum. The bacterium is usually found worldwide in coastal or estuarine water, sediments, and a variety of seafood such as shrimp, fish and oysters (Dalsgaard et al. 1996; Phillips et al. 2017). Consumption of contaminated raw or undercooked seafood causes severe to life-threatening infection in susceptible individuals that impair their immune system, and even more commonly in those with impaired liver function. The spectrum of *V. vulnificus*-associated disease varies from gastroenteritis to primary septicemia (Chuang et al. 1992; Hlady et al. 1996; Strom et al. 2000). These symptoms are commonly observed within 12 hours to 21 days. The primary septicemia is the most lethal with an average mortality rate exceeding 50% and death can occur within one to two days after the first signs of illness (Jones et al. 2009; Horseman et al. 2011). Infection with *V. vulnificus* also causes skin and soft-tissue infection that are resulted from handling contaminated raw seafood or from exposure of open wounds to water containing the bacterium. Moderate wound infection occurs in patients without obvious risks, but severe wound infection is often characterized by cellulitis, ecchymosis and bullae which can progress to necrotizing fasciitis at the infection site. The mortality from the wound infection is lower than primary septicemia, 17% (Horseman et al. 2011). Although *V. vulnificus*-related infections are rare, the bacterium has highly economic impact of all food related diseases in the United States (Phillips et al. 2017). Unique aspects of the infections caused by *V. vulnificus* are that most cases occur in persons over the age of 50, and, based on data compiled by the Food and Drug Administration, of 249 cases that occurred in this country over the last 10 years, 85% of the individuals who developed endotoxic shock from *V. vulnificus* infection were males (Merkel et al. 2001).

Although the role of gender in *V. vulnificus*-induced endotoxic shock and death is unclear, the major female hormone, estrogen, appears to be a protective material after exposure to endotoxin.

1.2. Virulence factors of *V. vulnificus*

1.2.1. Capsular polysaccharide (CPS) and Lipopolysaccharide (LPS)

V. vulnificus expresses an extracellular acidic polysaccharide capsule on its cell surface and uses the capsular polysaccharide (CPS) to avoid phagocytosis by macrophages (Linkous et al. 1999; Strom et al. 2000). The presence of a capsule is involved in colonies morphology; encapsulated isolates have an opaque colonial morphology but undergo a reversible phase variation to a translucent colony phenotype that is correlated with reduced or patchy expression of CPS (Wright et al. 1999). Unencapsulated mutants exhibit attenuated mortality in mouse models (Smith et al. 2003).

Lipopolysaccharide (LPS) is a potent mediator of endotoxin shock through the over-production of tumor necrosis factor (TNF) in host. In one study, it was demonstrated that the LPS extracted from *V. vulnificus* decreases heart rate and arterial pressure, followed by death in a rat model (McPherson et al. 1991). Low-density lipoprotein (LDL) appears to protect *V. vulnificus* LPS-induced lethality (Park et al. 2007). Injection of LDL prior to LPS increased mouse survival and delayed the LPS-induced lethality.

1.2.2. Hemolysin and RTX toxin

VvhA is an extracellular hemolysin/cytolysin encoded by *vvhA*, which induce cytolysis and death of erythrocytes in host through pore formation in the cellular membrane (Kim et al. 1993). Hemolysin causes a variety of pathological effects including tissue necrosis, fluid accumulation in intestinal tissue, increased vascular permeability and apoptosis of endothelial cells (Gray et al. 1987; Lee et al. 2005). However, inactivation

of the gene *vvhA* did not affect the LD_{50} of *V. vulnificus* in mouse model, suggesting that hemolysin is not solely implicated in the lethality and tissue damage (Wright et al. 1991).

RtxA1 is a multifunctional-autoprocessing RTX (MARTX) toxin encoded by *rtxA1*, which has highly sequence homology with its ortholog in *V. cholerae*. The RtxA1 is composed of repeated structural subunits and forms pores in host cell membranes. The deletion mutation of *rtxA1* gene leads to stop releasing MARTX toxin and decrease intestinal epithelial tissue damage (Jeong et al. 2012). Recently, Collaboration between RtxA1 and VvhA has been demonstrated to play an additive role in causing necrosis and intestinal tissue damage (Jeong et al. 2012).

1.2.3. Motility

Flagellum-mediated motility is a crucial virulence factor, facilitating pathogenic bacteria not only survival in the environment, but also host adhesion and colonization (Ottemann et al. 1997). The transposon insertion *V. vulnificus* mutant at the *flgC* gene encoding a flagellar basal body showed a decreased cytotoxicity to HeLa cells (Kim et al. 2003). Flagellum-deficient *flgE V. vulnificus* mutant also decreased adhesion to INT-407 cells (Lee et al. 2004).

2. Bacterial motility

To adapt and survive successfully to the environmental cues and changes, bacteria have to make a right decision to stay or move. Bacterial motility allows them to directly move toward favorable or away from unfavorable environments. The flagella are semi-rigid helical propellers and highly efficient means of bacterial locomotion. Flagellated bacteria can propel themselves in liquid (swimming) or move over and colonize surfaces (swarming). While swimming motility refers to the movement of individual

cells, swarming is the movement of a group of bacteria, suggesting that the swarming motility plays a key role within microbial communities and biofilm (Kearns 2010). Bacteria that swarm on surfaces display a hyperflagellated or hyperelongated morphology because of surface friction or high viscosity. Some motile bacteria such as *Myxococcus*, *Neisseria*, and *Pseudomonas* depend on type IV pili, which are extended and retracted into the cell upon attachment to the surface, generating a pulling movement (twitching). Notably, flagellar motility is approximately one thousand times faster than twitching motility (Mauriello et al. 2010). For example, *Vibrio* species swim in liquid environments at speeds as fast as 60 μm/s by using their single flagellum (McCarter 2001).

2.1. Bacterial flagella

The bacterial flagellum is a filamentous organ which acts as a helical propeller and facilitates efficient locomotion (Xie et al. 2011). The complete flagellar machinery is composed of three major parts: the basal body (the engine), the hook and filament structures extending towards the extracellular space. The basal body contains a cytoplasmic cup-like structure (C-ring), a flagellar type III secretion system (fT3SS), a membrane-embedded part and rod. The bacterial flagellum can be powered by the electrochemical gradient of the coupling ion (proton or sodium). Whereas the proton motors of *Escherichia coli* and *Salmonella typhimurium* spin up to 300 Hz, the sodium motor of *V. alginolyticus* can rotate remarkably faster, up to 1,700 Hz (Magariyama et al. 1994; Chen et al. 2000). Although the flagellar structure, function of the flagella genes, and their regulatory mechanisms are overall conserved and well characterized in motile bacteria, the flagellation patterns such as location and number are diverse among bacterial species. Well-characterized examples of the flagellation patterns are peritrichous (many flagella along the lateral side, e.g. *Bacillus subtilis*, *E. coli*), monotrichious

(a single flagellum at one pole, e.g. *Caulobacter*, *Pseudomonas*, *Shewanella*, *Vibrio*), amphitrichous (bipolar flagella, e.g. *Campylobacter*), and lophotrichous (some flagerlla at one pole, e.g. *Helicobacter*) (Schuhmacher et al. 2015).

2.1.1. Flagellar gene regulation

From an architectural perspective, more than 50 gene products need to come together in a highly ordered flagellar assembly process which is controlled by elegant transcriptional mechanisms. This scheme of gene expression control temporally and tightly couples to assembly process and has been well-characterized in the peritrichously flagellated *Salmonella* (Chilcott et al. 2000). In *Vibrio* species, the pyramid of gene expression for polar flagellar synthesis is more complex and possesses four classes (Figure 1). Genes in each class have to be functional in order for expression of the subsequent class to occur. In *Vibrio*, the only class I gene product, FlrA, activates class II genes that encode structural components and transcription factors such as FlhF, FlhG, and FliA. The class II transcription factors regulate the expression of class III and IV genes, encoding hook, basal body, and additional flagellins, respectively. Two sigma factors are involved in the regulation (Kim et al. 2000). σ^{54} (RpoN) controls class 2 and 3 operons, and σ^{28} (FliA) controls class 4 operons. Interestingly, it was determined that FlhG and FlhF regulate class I and class III genes transcription, respectively, as well as number of the polar flagellum in *Vibrio* species (Correa et al. 2005; Kusumoto et al. 2008; Yamaichi et al. 2012).

2.1.2. Flagellar assembly

Flagellar assembly starts at the inner structure of the basal body then proceeds to the outer ones (Figure 1). The first structure that is built is the MS ring which is the core structure of the rotor and is embedded in the

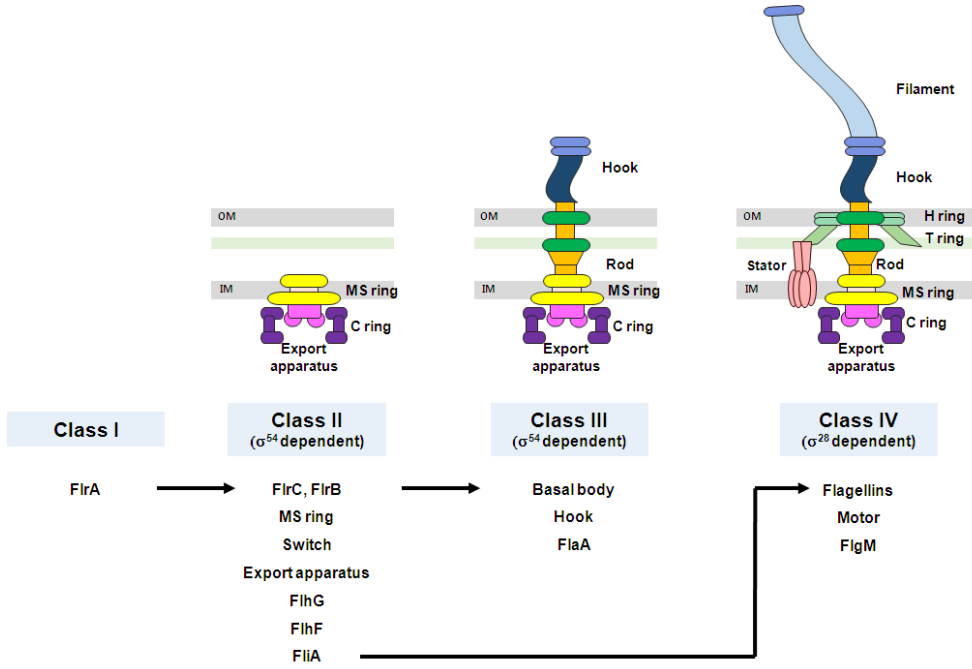

Figure 1. Hierarchy of polar flagellum gene expression in *Vibrio*, **based on previous reports.** (McCarter 2001; Correa et al. 2005)

cytoplasmic membrane (Ueno et al. 1992). The C ring attaches to the cytoplasmic portion of MS ring, and then the flagellum-specific export apparatus is assembled within the MS ring (Francis et al. 1994). After the export apparatus is completely established, the structural basal body proteins which are expressed from the class II genes are secreted through the export apparatus in the order described below. The proximal and distal rods are assembled on the MS ring (Homma et al. 1990). Then the P ring forms around the distal rod, followed by L-ring formation (Chevance et al. 2007). About 120 copies of FlgE proteins assemble the hook, and hook elongation proceeds to the well-controlled length of 55±6 nm by FliK (Hirano et al. 1994). After the hook reaches to a reasonable length, FlgD, the hook capping protein, is dissociated from the tip of the hook, and then replaced by the hook associated proteins, FlgK and FlgL (Homma et al. 1985). Finally, flagellins are polymerized to form the bacterial flagellum only in the presence of the filament cap protein, FliD (Yonekura et al. 2000).

2.1.3. Structural diversity of the hook basal body (HBB)

The core structure components and organization are well conserved in diverse bacterial species (Francis et al. 1994; Terashima et al. 2013; Zhu et al. 2013). For example, the motor structures are similarly embedded in the cytoplasmic and outer membranes and possess a MS ring, C ring, rod, export apparatus, and L/P rings. Interestingly, the HBB of *Vibrio* species contains three additional rings, the T, H, and O rings which are the divergent and symmetric structures surrounding the conserved core structure (Zhu et al. 2013; Minamino et al. 2015). The T ring, which is composed of MotX and MotY, facilitates efficient assembly of the torque generator, the PomAB stator complex. The H ring is located at the top of the T ring, and FlgT is the main protein component of the H ring. Recently, cryoelectron tomography and subtomogram analysis revealed that the O ring is associated with a

band of the outer membrane at 90° and might play important roles in sheath formation (Zhu et al. 2017).

2.1.4. Landmark system for localization of flagella

2.1.4.1. Regulation of flagellation patterns by FlhF and FlhG

In diverse bacteria species, two regulatory proteins, FlhF and FlhG (synonyms: YlxH, FleN, MotR, MinD2), are essential for establishing specific arrangement and quantity of flagella (Kusumoto et al. 2008; Schuhmacher et al. 2015). FlhF is a GTPase protein and is similar to the signal recognition particle receptor FtsY. Its GTPase motif influences the intracellular location, and GTPase activity is stimulated through interactions with FlhG. FlhG is an ATPase protein and is similar to MinD, a cell division regulator in prokaryotes.

2.1.4.1.1. The role of FlhF and FlhG in monotrichous flagellation

Monotrichious bacteria such as *Vibrio* and *Pseudomonas* species have a single polar flagellum, so flagellar structural components have to localize to a single cell pole. Two proteins, FlhF and FlhG, are involved in this process (Kusumoto et al. 2008; Kazmierczak et al. 2013). *flhF* deleted mutant strain does not have a polar flagellum, whereas overexpression of FlhF in *Vibro* and *Pseudomonas* species increased the number of polar flagella leading to motility defect. In contrast to FlhF, overproduction of FlhG causes a decrease in flagellation, and depletion of *flhG* increases the number of flagella. These results suggest that FlhF and FlhG execute antagonistically, acting as positive and negative regulators, respectively.

2.1.4.1.2. The role of FlhF and FlhG in amphitrichous, lophotrichous and peritrichous flagellation

In amphitrichously flagellated *C. jejuni*, depletion of *flhF* produces no

flagella or just a single flagellum at one pole (Balaban et al. 2009; Balaban et al. 2011). On the other hands, deletion of FlhG leads to less motile bacteria, which are multi-flagellated at least at one cell pole. *H. pylori*, the lophotrichous-flagellated bacterium, exhibits several flagella at one cell pole. Its *flhG* (*ylxH*) mutant is nonmotile and does not possess flagella (van Amsterdam et al. 2004). *B. subtilis* exhibits approximately 25 peritrichous flagella per cell that are absent from the cell poles. Deletion of either *flhF* or *flhG* in *B. subtilis* leads to mislocalization of flagella (Guttenplan et al. 2013).

2.1.4.2. The landmark system in *Vibrio* (HubP)

HubP, hub of the pole, was identified as a polar landmark protein conserved in all *vibrionaceae/photobacteriacea* that modulates polar localization of three ParA-like proteins such as ParA1, ParC, and FlhG (Yamaichi et al. 2012). It is a single-pass transmembrane protein whose N and C terminal domains show similarity to FimV, a positive regulator of type IV pilus formation in *P. aeruginosa* (Semmler et al. 2000; Wehbi et al. 2011). HubP has an N-terminal periplasmic LysM domain which binds to peptidoglycan in *P. aeruginosa* and is required for polar localization in *V. cholera* and *S. putrefaciens* CN-32 (Rossmann et al. 2015). Its C-terminal cytoplasmic region is comprised of 10 copies of an imperfect 46-amino-acid repeat in *V. cholera* (Yamaichi et al. 2012). HubP is well conserved in *Vibrionaceae/Photobacteriaceae*, and several other gamma-proteobacteria (Yamaichi et al. 2012; Rossmann et al. 2015; Takekawa et al. 2016). Fluorescence microscopy demonstrated that deletion of *hubP* results in delocalization of client proteins, suggesting that HubP is a determinant of polar protein localization. HubP interacts directly with ParA1, which is involved in chromosome partitioning (Yamaichi et al. 2012), and the ParA-like protein, FlhG, which regulates flagellar number and positioning

(Yamaichi et al. 2012; Takekawa et al. 2016). Deletion of *hubP* does not strongly affect flagellar number and positioning in *V. cholerae*. In the absence of HubP, however, *V. alginolyticus* cells increase the number of flagella. HubP does not directly interact with, but recruits ParC which is the ParA homolog and required for polar localization of chemotactic machinery (Ringgaard et al. 2014).

2.2. Chemotaxis

The ability of motile bacteria to recognize chemical gradient and direct themselves toward favorable or away from unfavorable environmental stimuli provides cells with a survival advantage. This behavior, called chemotaxis, is achieved by modulating the direction or speed of flagellar rotation (Boin et al. 2004; Butler et al. 2005). A sophisticated signal transduction system which consists of signal transducer proteins, a histidine kinase, a response regulator, and an adaptor protein passes input signals on to the flagellar motor. Chemoeffectors are detected by the transmembrane chemosensory proteins termed “methyl-accepting chemotaxis proteins” (MCPs). This input signal is transmitted through the cytoplasmic adaptor protein, CheW, to the histidine kinase, CheA (Gegner et al. 1992; Schuster et al. 1993). Upon recognition of a decrease in attractant or increase in repellant, the MCPs induce CheA autophosphorylation. Phosphorylated CheA transfer its phosphate to the response regulator, CheY, which diffuses throughout the cytoplasm. CheY-P binds to the flagellar switch protein FliM causing a switch from counterclockwise to clockwise rotation, resulting in movement toward more favorable conditions (Bren et al. 2001). Adaptation to a stable background level of attractant is accomplished by modulating the methylation state of the MCPs using two proteins, a constitutively active methyltransferase CheR (Springer et al. 1977) and a methylesterase CheB, whose activity is stimulated after phosphorylation by CheA-P (Yonekawa et

al. 1983).

2.2.1. Chemotaxis in *V. cholerae*

Chemotaxis has been extensively studied in the peritrichously flagellated bacteria *E. coli* (Armitage 1999; Stock et al. 2002). *E. coli* encodes four MCPs and single copies of each chemotaxis component. However, many other bacterial species possess multiple paralogues of each component, often organized into independent system. *V. cholerae* is no exception and has 68 putative chemotaxis proteins, including multiple copies of the *che* genes and 45 MCP-like proteins (Butler et al. 2005). The most of the genes encoding MCP-like proteins are found throughout the genome while the *che* genes are found in three clusters (I, II and III) (Boin et al. 2004). It has been reported that only genes located in *che* cluster II are important in *V. cholerae* chemotaxis and the other systems might control other physiological functions. In a recent study, cluster I chemotaxis proteins were observed to localize to membrane regions under microaerobic conditions, suggesting that cluster I might be involved in sensing during oxygen depletion (Hiremath et al. 2015). Expression of *che* cluster III is induced by carbon starvation and is positively regulated by global stress regulator, RpoS (Ringgaard et al. 2015).

3. The phosphoenolpyruvate: carbohydrate phosphotransferase system

3.1. Barcterial PTS

Solutes transfer across the cytoplasmic membrane proteins called transport system, and this requires an expenditure of energy and specific proteins. There are three categories of major transport systems in microbes; Ion driven transport system, ATP binding dependent system, and group translocation system. The group translocation of carbohydrates is mediated by bacterial phosphoenolpyruvate (PEP): carbohydrate phosphotransferase

system (PTS) which uses PEP to phosphorylate a number of hexoses including *N*-acetylmannosamine, glucose, mannose, glucosamine, and *N*-acetylglucosamine (Kundig et al. 1964). The PTS catalyzes the uptake of with a concomitant phosphorylation of numerous carbohydrates and regulates many metabolic functions of the cell including transport of particular sugars. It is composed of two general cytoplasmic proteins, enzyme I (EI) and the histidine-containing phosphocarrier protein (HPr), which are common to all PTS sugars, and various sugar-specific enzyme II (EII) complexes (Barabote et al. 2005). Each EII complex usually consists of two cytoplasmic domains, EIIA and EIIB, and one transmembrane domain, EIIC. The number and structure of the EII complexes vary between species while the amino acid sequences of EI and HPr are strongly conserved in all bacteria. EI and HPr mediate phosphoryl transfer from PEP to EII, which leads to the phosphorylation of a PTS sugar during its transport into cell. Specifically, EI, HPr and EIIA are phosphorylated at histidine and EIIB domains are phosphorylated at either cysteine or histidine depending on the particular transporter (Siebold et al. 2001).

3.2. PTS-mediated regulation in *E. coli*

3.2.1. Carbon catabolite repression

The preferential utilization of a certain carbon source over others has been observed in various model organisms. Carbon catabolite repression (CCR) is the phenomenon in which the presence of carbon source metabolizable rapidly, such as glucose, in the growth medium inhibits the gene expression and/or protein activity involved in the metabolism of alternative carbon sources. PTS sugars have been generally believed to be preferred over non-PTS sugars in various bacteria species (Deutscher et al. 2006; Gorke et al. 2008). If *E. coli* grows in a medium supplemented both glucose and lactose, it uses glucose preferentially until the glucose is

exhausted. Than after a short lag, growth resumes with lactose as the carbon source. This biphasic growth pattern shown in two carbon sources is called diauxic growth. The current model for the glucose preference over other sugars has been extensively studied in *E. coli*, and involves inducer exclusion and induction prevention (Gorke et al. 2008), both of which depends on the phosphorylation state of $EIIA^{Glc}$.

3.2.1.1. Inducer exclusion

When a PTS sugar is transported, $EIIA^{Glc}$ becomes predominately dephosphorylated, and interacts with and inhibits several non-PTS permeases such as lactose, maltose, and melibiose permease (Postma et al. 1993). The dephosphorylated $EIIA^{Glc}$ can also interact with and inhibit glycerol kinase. This phenomenon is called inducer exclusion, since the preferred substrate or one of its metabolic derivatives inhibits the entry of molecules that induce other metabolic systems (Postma et al. 1993).

3.2.1.2. Induction prevention

After glucose is exhausted in a medium, $EIIA^{Glc}$ is phosphorylated and then stimulates adenylate cyclase, an enzyme converting ATP into 3',5'-cyclic adenosine monophosphate (cyclic AMP; cAMP) (Park et al. 2006). Together with cAMP receptor protein CRP, cAMP is involved in the global regulation of numerous genes and operons required for the transport and/or metabolism of carbon sources. Because glucose leads to dephosphorylation of $EIIA^{Glc}$ during transport via the PTS, glucose transport results in a deactivation of adenylate cyclase, leading to a decrease in the cellular cAMP level and thus prevention of induction of many catabolic genes (Gorke et al. 2008). This phenomenon is termed induction prevention. Based on the inducer exclusion and induction prevention, $EIIA^{Glc}$ is regarded as the central processing unit of CCR in *E. coli* and other enteric bacteria

(Deutscher et al. 2006).

3.2.2. Interaction between adenylate cyclase and EIIA^{Glc}

In *E. coli*, mutants that lack any one constituent of the *pts* operon, EI, HPr, or EIIA^{Glc}, normally exhibit low rates of cAMP synthesis. These *in vivo* observations are attributed to a mechanism of adenylate cyclase (AC) regulation which is activated by phosphorylated EIIA^{Glc} (Peterkofsky et al. 1993). AC is composed of two domains, an N-terminal catalytic domain and a C-terminal regulatory domain (Roy et al. 1983). The C-terminal domain is required for glucose-specific regulation of AC. It has been demonstrated that both phosphorylated and unphosphorylated form of EIIA^{Glc} interacts directly with AC. However, experiments using a membrane-tethered form of AC (Tsr-AC) revealed that the C-terminal region of AC specifically interacts with EIIA^{Glc} and only the phosphorylated form of EIIA^{Glc} can stimulate the level of AC activity (Park et al. 2006).

3.3. PTS in *V. vulnificus*

Because simple sugars are present in the marine environment in submicromolar concentrations, marine bacteria have to uptake sugars through highly efficient transport systems such as the PTS. It has been known that the component proteins of the PTS are also highly conserved in enteric bacteria and crossreact with corresponding proteins with *E. coli*. Genetic organization of the PTS components in *V. vulnificus* is also similar with that in *E. coli*. For example, it possesses *ptsHIcrr* operon, which is encoding HPr, EI, and EIIA^{Glc}, and separated *ptsG* gene encoding EIIBC^{Glc}.

3.4. PTS-mediated regulation in *V. vulnificus*

3.4.1. Interaction between Vibrio insulin degrading enzyme (vIDE) and EIIA^{Glc}

Protein ligand fishing experiment revealed that $EIIA^{Glc}$ regulates the activity of a protease homologous to mammalian insulin-degrading enzymes by direct interaction. While specific interaction with the IDE is not dependent on the phosphorylation state of $EIIA^{Glc}$, only dephosphorylated form of $EIIA^{Glc}$ activates the peptidase activity of vIDE (Kim et al. 2010).

4. The aims of this study

In *E. coli*, the synthesis of flagella and hence swimming motility have been reported to be repressed in the presence of glucose, while flagellar motility is generated when the cells are cultivated either in the absence of glucose or in the presence of non-PTS sugars, such as glycerol or succinate (Adler et al. 1967; Dobrogosz et al. 1971). And it was also reported that its glucose-dependent repression could overcome by addition of exogenous cAMP (Yokota et al. 1970). It is explained by analogous phenomenon to catabolite repression which allows bacteria to adapt to a preferred carbon source. In *E. coli*, it is suggested that the phosphorylated $EIIA^{Glc}$ stimulates the level of AC activity, whereby the activation of AC determines the level of cAMP which affects flagellar assembly (Yokota et al. 1970; Park et al. 2006). The molecular mechanism governing this phenomenon, however, remains mostly unknown in other bacteria.

Bacterial species in which flagellar synthesis is known to be suppressed by glucose use the PTS system to transport glucose (Adler et al. 1967; Dobrogosz et al. 1971; Lawley et al. 2013). Because members of the family *Vibrionaceae* also take up glucose by group translocation via the PTS, I assumed that a glucose-specific PTS component may participate in regulation of flagellar motility. In this study, a novel mechanism for glucose PTS-dependent on-off switching of flagellar synthesis was identified using *V. vulnificus* as a model system.

Chapter II. Materials and Methods

1. Bacterial strains, plasmids, and culture conditions

Bacterial strains and plasmids used in this study are listed in Table 1. Details of the plasmid construction and oligonucleotides are described from 1.1 to 1.18 and Table 2. *V. vulnificus* strains were grown in Luria-Bertani medium supplemented with 2.5% NaCl (LBS) at 30°C and *E. coli* strains were cultured in LB medium at 37°C. To avoid medium acidification, bacterial cells were grown in 20 mM sodium phosphate-buffered LBS broth (pH 8.0) supplemented with 0.2% glucose (Gardner et al. 2003). The following supplements were added if necessary: kanamycin, 200 μg ml^{-1} for *V. vulnificus* and 50 μg ml^{-1} for *E. coli*; ampicillin, 20 μg ml^{-1} for *V. vulnificus* and 100 μg ml^{-1} for *E. coli*; chloramphenicol, 2 μg ml^{-1} for *V. vulnificus* and 10 μg ml^{-1} for *E. coli*; isopropyl-β-D-1-thiogalactopyranoside (IPTG), 1 mM; L-arabinose, 0.02%. Constructions of the *fapA* and *hubP* deletion mutants were generated by allelic exchange using plasmid pDM4-fapA and pDM4-hubP, respectively, (see 1.1, 1.2 and Table 2) as described previously (Kim et al. 2015).

1.1. Construction of the pDM4-fapA plasmid and a *fapA* deletion mutant

The up- and down-stream regions of the *fapA* (*VVMO6_04547*) gene were amplified by PCR using primer pairs of JW001-JW002 and JW003-JW004, respectively. After digestion of the two PCR products, the XhoI-ApaI and ApaI-XbaI fragments, respectively, were cloned into the corresponding sites of the suicide vector pDM4 to generate the plasmid pDM4-fapA. To construct a *fapA* deletion mutant of the *V. vulnificus* MO6-24/O strain, the *E. coli* SM10 *λpir* strain carrying pDM4-fapA was conjugated with *V. vulnificus* MO6-24/O, and the transconjugants were selected. Integration was confirmed by PCR, and the exoconjugants were selected in LBS containing 8% sucrose. Deletion of *fapA* in the selected

colonies was confirmed by PCR.

1.2. Construction of the pDM4-hubP plasmid and a *hubP* deletion mutant

The up- and down-stream regions of the *hubP* (*VVMO6_00873*) gene were amplified by PCR using primer pairs of JY001-JY002 and JY003-JY004, respectively. After digestion of the two PCR products, the XhoI-ApaI and ApaI-XbaI fragments, respectively, were cloned into the corresponding sites of the suicide vector pDM4 to generate the plasmid pDM4-hubP. To construct a *hubP* deletion mutant of the *V. vulnificus* MO6-24/O strain, the *E. coli* SM10 *λpir* strain carrying pDM4-hubP was conjugated with *V. vulnificus* MO6-24/O, and the transconjugants were selected. Integration was confirmed by PCR, and the exoconjugants were selected in LBS containing 8% sucrose. Deletion of *hubP* in the selected colonies was confirmed by PCR.

1.3. Construction of plasmids pSY001 and pSY002 to overexpress $EIIA^{Glc}$

The plasmid pSY001 was constructed by PCR amplification of the *VVMO6_02250* gene encoding $EIIA^{Glc}$ from the chromosomal DNA of *V. vulnificus* MO6-24/O using the primers JW005 and JW006. The PCR fragment was digested with BamHI and SalI and inserted into the corresponding sites of pETDuet-1 (Novagen). Similarly, using a primer pair of JW007 and JW008, the *VVMO6_02250* gene was also cloned into NdeI and BamHI sites of the pET24a (Novagen) to generate pSY002.

1.4. Construction of plasmids pSY003 and pSY004 to overexpress FapA

The *fapA* gene was amplified by PCR from *V. vulnificus* MO6-24/O using a primer pair of JW009 and JW010. The PCR product was digested

with NdeI and BamHI and inserted into the corresponding sites of plasmids pET24a and pET28a (Novagen) to generate pSY003 and pSY004, respectively.

1.5. Construction of plasmids pSY005 and pSY006 to overexpress GFP and GFP-FapA, respectively

The *gfp* gene was amplified by PCR with the primers JW011 and JW012. The PCR product was cloned into EcoRI site of pJK1113 to generate pSY005. The *fapA* gene was amplified from the chromosomal DNA of *V. vulnificus* MO6-24/O by PCR using the primers JW013 and JW014. The PCR fragment was digested with XbaI and SalI and inserted into the corresponding sites of the pSY005 plasmid to generate pSY006 expressing the GFP-FapA fusion protein.

1.6. Construction of plasmids pSY007, pSY008, and pSY009 to overexpress RFP (pSY007, 008) and FlhF-RFP (pSY009)

The *rfp* gene was amplified by PCR with the primers JW015 and JW016. After digestion with SphI, the PCR product was cloned into the corresponding site of pJK1113 to generate the plasmid pSY007. To construct pSY008, the *bla* gene in pSY007 was replaced with a chloramphenicol resistance marker. First, the *cat* gene was amplified from pDM4 by PCR with the primers JW017 and JW018, and the entire sequence except the *bla* gene in pSY007 was amplified by inverse PCR using the primers JW019 and JW020. These two PCR products having 15-bp complementary sequences at both ends were then combined by EZ-Fusion™ Cloning kit (Enzynomics), resulting in pSY008. To construct the plasmid pSY009, the *VVMO6_00833* gene encoding the FlhF protein was amplified from the chromosomal DNA of *V. vulnificus* MO6-24/O using the primers JW021 and JW022. Similarly, this PCR product and the linearized

PCR product of pSY008 amplified by inverse PCR using the primers JW023 and JW024 were combined using EZ-Fusion™ Cloning kit (Enzynomics) to generate the pSY009 plasmid expressing the FlhF-RFP fusion protein.

1.7. Construction of pRK415-based expression vector for EIIA^{Glc} and EIIA^{Glc}(H91A), pSY010 and pSY011, respectively

The *VVMO6_02250* gene encoding EIIA^{Glc} was amplified by PCR from *V. vulnificus* MO6-24/O using the primers JW008 and JW025. The PCR product was digested with PstI and BamHI and then inserted into the corresponding sites of pRK415 to generate the plasmid pSY010. The pRK415-based expression vector pSY011 for the expression of EIIA^{Glc}(H91A) was generated with an additional mutagenic primer pair (JW026 and JW027) covering the region coding for the phosphorylation site His91 using the QuickChange method (Stratagene).

1.8. Construction of pJK1113-based expression vector for EIIA^{Glc} and EIIA^{Glc}(H91A), pSY012 and pSY013, respectively

Using a primer pair of JW028 and JW029, the *VVMO6_02250* gene and the mutated version of the *VVMO6_02250* gene were amplified by PCR from pSY010 and pSY011, respectively. Each PCR product and a linearized product of pSY008 amplified by inverse PCR using the primers JW023 and JW030 were combined by the EZ-Fusion™ Cloning kit (Enzynomics), resulting in the plasmids pSY012 and pSY013, respectively.

1.9. Construction of the plasmid pSY014 to overexpress GFP-FapA

The DNA fragment covering *gfp-fapA* was amplified by PCR from pSY006 using the primers JW031 and JW032. This PCR product and a linearized product of pRK415 through digestion with PstI and BamHI were

combined by the EZ-Fusion™ Cloning kit (Enzynomics), resulting in the plasmid pSY014.

1.10. Construction of the plasmid pSY015 to overexpress FapA

The *fapA* gene was amplified by PCR from *V. vulnificus* MO6-24/O using the primers JW033 and JW034. The PCR product was digested with EcoRI and SalI and inserted into the corresponding sites of pJK1113 to generate pSY015.

1.11. Construction of the plasmid pRK-P_1-FapA

The DNA fragment containing the *fapA* gene and its P_1 promoter region located within the upstream gene VVMO6_04548 was amplified by PCR from *V. vulnificus* MO6-24/O genomic DNA using the primers JW035 and JW036. The PCR product was digested with BamHI and PstI and inserted into the corresponding sites of pRK415 to generate pRK-P_1-FapA.

1.12. Construction of the plasmid pRK-FapA

The DNA fragment containing the *fapA* open reading frame was amplified by PCR from *V. vulnificus* MO6-24/O genomic DNA using the primers JW037 and JW010. The PCR product was digested with PstI and BamHI and inserted into the corresponding sites of pRK415 to generate pRK-FapA.

1.13. Construction of the plasmid pSY016 to overexpress HubP 658

The *hubP* gene was amplified by PCR from *V. vulnificus* MO6-24/O using a primer pair of JY005 and JY006. The PCR product was digested with NdeI and XhoI and inserted into the corresponding sites of plasmids pET24a (Novagen) to generate pSY016 expressing HubP 658.

1.14. Construction of the plasmid pSY017, pSY018, and pSY019 to overexpress HubP truncation mutants

To construction of each HubP truncation mutants (HubP 1267, 1561, and 1719) expression vector, the *hubP* gene were amplified by PCR using primer pairs of JY006-JY007, JY006-JY008 and JY006-009, respectively. The PCR product was digested with NdeI and XhoI and inserted into the corresponding sites of plasmids pETDuet-1 (Novagen) to generate pSY017, pSY018 and pSY019, respectively.

1.15. Construction of the plasmid pSY020 and pSY021 to overexpress HubP

The *hubP* gene was amplified by PCR with the primers JY010 and JY012. After digestion with NcoI and SalI, the PCR product was cloned into the corresponding site of pJK1113 to generate the plasmid pSY020. To construct pSY021, the *bla* gene in the pSY020 was replaced with a chloramphenicol resistance marker. First, the *cat* gene was amplified from pDM4 by PCR with the primers JW017 and JW018, and the entire sequence except the *bla* gene in the pSY020 was amplified by inverse PCR using the primers JW019 and JW020. These two PCR products having 15-bp complementary sequences at both ends were then combined by EZ-Fusion™ Cloning kit (Enzynomics), resulting in the pSY021.

1.16. Construction of the plasmid pSY022 and pSY023 to overexpress HubP-RFP and HubP 658-RFP, respectively

The full-length *hubP* gene and the DNA fragment covering *hubP 658* were amplified by PCR using primer pairs of JY013-JY015 and JY014-JY015, respectively. These PCR products and the linearized PCR product of pSY008 amplified by inverse PCR using the primers JW023 and JW024 were combined using EZ-Fusion™ Cloning kit (Enzynomics) to generate

the pSY022 and pSY023 plasmids expressing the HubP-RFP and HubP 658-RFP fusion protein, respectively.

1.17. Construction of the plasmid pSY024, pSY025 and, pSY026 to overexpress HubP truncation mutants

To construct of each HubP truncation mutant (HubP Δ1726, Δ1269, and Δ665) expression vector, linearized PCR products of pSY021 were amplified by inverse PCR using primer pairs of JY016-JY019, JY017-JY019, and JY018-JY019, respectively. Each linearized PCR product was recombined by the EZ-Fusion™ Cloning kit (Enzynomics), resulting in plasmids pSY024 expressing the HubP Δ1726, pSY025 expressing the HubP Δ1269, and pSY026 expressing the HubP Δ665.

1.18. Construction of the plasmid pSY027, pSY028 and, pSY029 to overexpress HubP truncation mutants

The *hubP* gene was amplified by PCR with the primers JY011 and JY012. After digestion with NcoI and SalI, the PCR product was cloned into the corresponding site of pJK1113 to generate the plasmid pSY027. To construct pSY028, the *bla* gene in the pSY027 was replaced with a chloramphenicol resistance marker. First, the *cat* gene was amplified from pDM4 by PCR with the primers JW017 and JW018, and the entire sequence except the *bla* gene in the pSY027 was amplified by inverse PCR using the primers JW019 and JW020. These two PCR products having 15-bp complementary sequences at both ends were then combined by EZ-Fusion™ Cloning kit (Enzynomics), resulting in the pSY028. To construct pSY029, linearized PCR product of the pSY028 was amplified by inverse PCR using primers JY017 and JY019. It recombined by the EZ-Fusion™

Cloning kit (Enzynomics), resulting in the plasmid pSY029 expressing the HubP 658-1267.

Table 1. Strains and plasmids used in this study

Strains or plasmids	Genotypes and/or descriptions	Reference or source
Strains		
V. vulnificus		
MO6-24/O	Wild-type, Clinical isolate	(Wright et al. 1990)
MO6-24/O *ΔfapA*	MO6-24/O with *ΔfapA*	This study
MO6-24/O *ΔhubP*	MO6-24/O with *ΔhubP*	This study
MO6-24/O *Δcrr*	MO6-24/O with *Δcrr*	Gift from KH Lee
MO6-24/O *Δcya*	MO6-24/O with *Δcya*	Gift from KH Lee
MO6-24/O *ΔflhF*	MO6-24/O with *ΔflhF*	Gift from SH Choi (Kim et al. 2012)
E. coli		
ER2566	F^- λ^- *fhuA2* [*lon*] *ompT lacZ*::*T7* gene 1 *gal sulA*11 Δ(*mcrC-mrr*)114::IS10 R(*mcr-*73::miniTn10-TetS)2 R(*zgb*-210::Tn10)(TetS) *endA1* [*dcm*]	New England Biolabs
BL21(DE3) pLysS	F^- *ompT gal dcm lon hsdSB*(rB- mB-) λ (DE3) pLysS(Cm^r)	Novagen
SM10 λ*pir*	*thi-1 thr leu tonA lacY supE recA*::RP4-2-Tc::Mu *λ pir*, OriT of RP4, Km^r; conjugational donor	(Miller et al. 1988)
Plasmids		
pDM4	Suicide vector for homologous recombination into *V. vulnificus* chromosome, OriR6K, Cm^r	(Milton et al. 1996)
pET24a		Novagen
pET28a		Novagen
pETDuet-1		Novagen
pJK1113	pBAD24 with *oriT* of RP4 and *nptI*, P_{BAD}; Km^r, Ap^r	(Lim et al. 2014)
pRK415	Broad host range vector, IncP *ori*, *oriT* of RK2, P_{lac}; Tc^r	(Keen et al. 1988)
pDM4-fapA	pDM4-based suicide vector for deletion of *fapA*, Cm^r	This study
pDM4-hubP	pDM4-based suicide vector for deletion of *hubP*, Cm^r	This study
pSY001	pETDuet-1-based expression vector for His_6 tagged-$EIIA^{Glc}$, Ap^r	This study
pSY002	pET24a-based expression vector for $EIIA^{Glc}$,	This study

	Km^r	
pSY003	pET24a-based expression vector for FapA, Km^r	This study
pSY004	pET28a-based expression vector for His_6 tagged-FapA, Km^r	This study
pSY005	pJK1113-based GFP fusion vector, Km^r, Ap^r	This study
pSY006	pSY005-based expression vector for GFP-FapA, Km^r, Ap^r	This study
pSY007	pJK1113-based RFP fusion vector, Km^r, Ap^r	This study
pSY008	pJK1113-based RFP fusion vector, Km^r, Cm^r	This study
pSY009	pSY008-based expression vector for FlhF-RFP, Km^r, Cm^r	This study
pSY010	pRK415-based expression vector for $EIIA^{Glc}$, Tc^r	This study
pSY011	pRK415-based expression vector for $EIIA^{Glc}$ (H91A), Tc^r	This study
pSY012	pJK1113-based expression vector for $EIIA^{Glc}$, Km^r, Cm^r	This study
pSY013	pJK1113-based expression vector for $EIIA^{Glc}$ (H91A), Km^r, Cm^r	This study
pSY014	pRK415-based expression vector for GFP-FapA, Tc^r	This study
pSY015	pJK1113-based expression vector for FapA, Km^r, Ap^r	This study
pSY016	pET24a-based expression vector for HubP 658, Km^r	This study
pSY017	pETDuet-1-based expression vector for HubP 1267, Ap^r	This study
pSY018	pETDuet-1-based expression vector for HubP 1561, Ap^r	This study
pSY019	pETDuet-1-based expression vector for HubP 1719, Ap^r	This study
pSY020	pJK1113-based expression vector for HubP, Km^r, Ap^r	This study
pSY021	pJK1113-based expression vector for HubP, Km^r, Cm^r	This study
pSY022	pSY008-based expression vector for HubP-RFP, Km^r, Cm^r	This study
pSY023	pSY008-based expression vector for HubP 658-RFP, Km^r, Cm^r	This study
pSY024	pJK1113-based expression vector for HubP Δ1726, Km^r, Cm^r	This study
pSY025	pJK1113-based expression vector for HubP Δ1269, Km^r, Cm^r	This study

pSY026	pJK1113-based expression vector for HubP Δ665, Km^r, Cm^r	This study
pSY027	pJK1113-based expression vector for HubP 658, Km^r, Ap^r	This study
pSY028	pJK1113-based expression vector for HubP 658, Km^r, Cm^r	This study
pSY029	pJK1113-based expression vector for HubP 658-1267, Km^r, Cm^r	This study
pRK-FapA	pRK415-based expression vector for FapA driven by the *lac* promoter, Tc^r	This study
pRK-P_1-FapA	pRK415-based expression vector for FapA driven by the P_1 promoter, Tc^r	This study

[a] Cm^r , chloramphenicol-resistant; Km^r , kanamycin-resistant; Ap^r , ampicillin-resistant; Tc^r , tetracycline-resistant.

Table 2. Oligonucleotides used in this study

Name	Oligonucleotide sequence (5'–3')*	Use(s)
JW001	CTATTGACCTCGAGACAGAGAATTTTCTTG (XhoI)	Construction of pDM4-fapA
JW002	AACTCAGGGCCCTAGAAGCAACGGAAAAAG (ApaI)	
JW003	GCAAAAGAGAATAATCGGGCCCACATCACT (ApaI)	
JW004	TTGAGTTTCTAGAAGGGCAATCGATCATCA (XbaI)	
JW005	GAGCAGGATCCAATGGGTCTGTTTGACAAA (BamHI)	Construction of pSY001
JW006	TGCAAGTCGACTGCTATCTTAGGTTGCTCA (SalI)	
JW007	GCATGACCATATGGGTCTGTTTGACAAACT (NdeI)	Construction of pSY002
JW008	GCTAACTAAGGATCCATTACTTAGTTACGCG (BamHI)	
JW009	GACCGTCCATATGTGGAAACTCTGCCTTTC (NdeI)	Construction of pSY003, pSY004, and pRK-FapA
JW010	ACGAGTTGGATCCTCTATCTCTAACTCGCT (BamHI)	
JW011	GCCCGTGAATTCACATGAGTAAAGGAGAAG (EcoRI)	Construction of pSY005
JW012	CGCAGCGAATTCCGGGCCCAATTTGTATAG (EcoRI)	
JW013	TAGTAAGCGACCGTCTAGATATGTGGAAAC (XbaI)	Construction of pSY006
JW014	GTCCAAAGTCGACTTAGATCATCTATCTCT (SalI)	
JW015	CATATTGCATGCATGGTGTCTAAGGGCGAAG (SphI)	Construction of pSY007
JW016	GTCGACAGCATGCCTCAATTAAGTTTGTGCCC (SphI)	
JW017	ATTGAAAAAGGAAGAGTATGGAGAAAAAAATCACT GGATATACCACCG	Construction of pSY008, pSY021 and pSY028
JW018	GTAAACTTGGTCTGACAGTTACGCCCCGCCCTGCCA CTCATC	
JW019	CATACTCTTCCTTTTTCAATATTATTGAAGC	
JW020	GTAACTGTCAGACCAAGTTTACTCATATATAC	
JW021	TGGGCTAGCAGGAGGAATTCATGTTGAAAATAAAAC GATTTTTTGCC	Construction of pSY009
JW022	GATCCCCGGGTACCATGGTGCGAGAATCCTTCGTTGT CACTGTTC	
JW023	GAATTCCTCCTGCTAGCCCAAAAAAACGG	Construction of pSY009, pSY022 and pSY 023
JW024	CACCATGGTACCCGGGGATCCTCTAGAGTC	
JW025	CTAAACCTTAGGAGCACTGCAGAATGGGTC (PstI)	Construction of pSY010 and pSY011
JW026	GTGTCGATACCGAAGGCAACAAACAGTTCAAC	
JW027	GTTGAACTGTTTGTTGCCTTCGGTATCGACAC	
JW028	TGGGCTAGCAGGAGGAATTCAGAATGGGTCTGTTTG ACAAACTTAAG	Construction of pSY012 and

JW029	AAACAGCCAAGCTTGCATGCCATTACTTAGTTACGC GTAGAACTG	pSY013
JW030	GCATGCAAGCTTGGCTGTTTTGGCG	
JW031	CGCCAAGCTTGCATGCCTGCAGGATGAGTAAAGGAG AAGAACTTTTCACTGG (PstI)	Construction of pSY014
JW032	GAGCTCGGTACCCGGGGATCCCTACACTGCGACGTC CTCTTCTTCTAAGG (BamHI)	
JW033	TAGTAAGCGGAATTCTATATGTGGAAACTC (EcoRI)	Construction of pSY015
JW034	GTCCAAAGTCGACTTAGATCATCTATCTCT (SalI)	
JW035	CCGATTTACGCGGGATCCTGAAAGGCGTAG (BamHI)	Construction of pRK-P_1-FapA
JW036	AACTCGCCTGCAGATCACTACACTGCGACG (PstI)	
JW037	TTGTAGTAAGCGACCTGCAGGATGTGGAAA (PstI)	Construction of pRK-FapA
JY001	AGCAGAGGCTCGAGTAGTCGTGATCGACAA (XhoI)	Construction of pDM4-hubP
JY002	GCATAGAGGGCCCAGCTCTGTGCTTAGTTA (ApaI)	
JY003	GATTAACGGGCCCTAGTTTCATTCTTAAGT (ApaI)	
JY004	TTCAGGGTAGTCTAGATCGACGAGATATAA (XbaI)	
JY005	AGCACCCATATGCTCGATGAATTACTGGAA (NdeI)	Construction of pSY016, pSY017, pSY018, and pSY019
JY006	AATTTCTAATCCTCAAGCCTCGAGCGATAA (XhoI)	
JY007	TGCAATGGCAGATCATATGGGCCCTTCACTCGCAG (NdeI)	
JY008	GCAGACCATATGGAGCCTTCTTACGATGCTCCGCTTG TAG (NdeI)	
JY009	GTTAACAAGCATATGCCGCATATCAATCCTTCTTCCTA TG (NdeI)	
JY010	CTAGCAGGAGGAATTCACCATGGCACGTCAAATTTT TAAGCGCCTGTTAGCC (NcoI)	Construction of pSY020 and pSY027
JY011	CTAGCAGGAGGAATTCACCATGGCACTCGATGAATT ACTGGAAAGCGCACC (NcoI)	
JY012	AAGCTTGCATGCCTGCAGGTCGACCTAACGGCCGTT AATCATATCAATGAG (SalI)	
JY013	TGGGCTAGCAGGAGGAATTCATCATGCGTCAAATTT TTAAGCGCCTGTTAGCC	Construction of pSY022 and pSY023
JY014	TGGGCTAGCAGGAGGAATTCATCATGCTCGATGAA TTACTGGAAAGCGCACC	
JY015	GATCCCCGGGTACCATGGTGCGAACGGCCGTTAATC ATATCAATGAG	
JY016	CATGCCTGCAGGTCGACCTAGGAAGAAGGATTGATA TGCGGCTTGTTAAC	Construction of pSY024, pSY025, pSY026 and pSY029
JY017	CATGCCTGCAGGTCGACCTAGCCATCTGCCATTGCA GACAG	
JY018	CATGCCTGCAGGTCGACCTAGCTTTCCAGTAATTCAT CGAGCAGATCGGTGC	
JY019	CTAGGTCGACCTGCAGGCATGCAAGCTTGGCTGTTT TG	

FlrA-F	GATTTTTCTCATCCTGTAGAACACCT	
FlrA-R	ATTAGGTGACGAACTTCTTGAATACCTA	
FleS-F	AGTGATTTACAGCGGTTATCTTCGTTA	
FleS-R	ATAACAACATATCGTTGACCTGTTTTTCC	
FlrC-F	GAAGATTTGTACTATCGTTTGAACGTTTTC	
FlrC-R	ACTACGTTATCAAGCTCACGCACATTAC	
FlaC-F	AGTGCTCTACAAGACGAAATTAACCGTATT	
FlaC-R	AATCTTTGTTTTTGCCATTTTCAGACTGG	
MotX-F	CTGTTGGTGTTGAGTGCTCCTTTTTCTA	qRT-PCR
MotX-R	TAAAGGAACTCGTACGCAGGTAGGTTAAT	
FliD-F	AAATCGGTGTGGAGTATGATAGACAGAG	
FliD-R	CTCTATTCGAGTCGAGAAAACACTCTTTA	
FlaF-F	GAAAGAATTGCCTTACAAGAAGAAATGACC	
FlaF-R	AATGTAACTGAAGCCACCCATATCAATAC	
FlaA-F	GTATCTCTATTGCACAGACTGCTGAAG	
FlaA-R	CGTTAAGGAGTTTGTTACCACCAAAAGAG	
FlaG-F	CATCCTACACATCGAACATCCAGCCTTACG	
FlaG-R	TCTCTTCTCTGTTGAGCTCCTGACGAGCTT	
FapA-F	ATTACCGCCAAATTGCCTGAGGCCGATTTG	qRT-PCR and RT-PCR
FapA-R	GGTGACTTTCATGCTGGCAAGCATGTCGTT	
04551-F	TGAATCGACACAAGCCTTCGGTGGATGTGA	RT-PCR
04550-R	TACGCGAGGAATCGCCGTTTGCAGAAAATG	
04549-F	GTGACCTTAGCAATAGAAGGGGCCTTTGGA	
04549-R	GCGCACTTGCGGTAAGGTGTTGATGATCTT	
04548-F	TGTAAGATGATGCTGAGCGATCTCGATGCC	
04548-R	ATCGCCAAAGGTTAGGCACTTACCGAAGGA	
5’-RACE P_1	GCCAAGGCATGCACAATTTCA	5’- RACE
5’-RACE P_2	AATCCACGGCCACCATAGGCGCCGGTGACT	

* Engineered restriction sites were underlined with the corresponding restriction enzyme shown in parentheses.

2. Purification of overexpressed proteins

N-terminal His-tagged proteins were overexpressed in *E. coli* BL21 (DE3) pLysS or ER2566 for pET vectors, and purified using TALON metal-affinity resin (Takara Bio) according to the manufacturer's instructions. The bound His-tagged proteins were eluted with 200 mM imidazole, and then chromatographed on a HiLoad 16/600 Superdex 75 pg column (GE Healthcare Life Sciences) equilibrated with buffer A (50 mM Tris-HCl, pH 7.5, containing 100 mM NaCl) to remove imidazole and increase purity (>98% pure). Proteins without a His-tag were overexpressed in *E. coli* BL21 (DE3) pLysS or ER2566 for pET vectors. Harvested cells were disrupted by three passages through a French pressure cell at 8,000 psi and centrifuged at 100,000 x *g* at 4°C for 40 min. The proteins were purified by ion exchange chromatography using a Mono Q 10/100 column (GE Healthcare Life Sciences) and gel filtration chromatography using a HiLoad 16/600 Superdex 75 pg column according to the method described for purification of vIDE (Kim et al. 2010). Insoluble HubP truncation mutants were overexpressed in *E coli* ER2566. Harvested cells were disrupted by three passages through a French pressure cell at 8,000 psi and centrifuged at 10,000 x *g* at 4°C for 5 min. The supernantant was centrifuged at 100,000 x *g* at 4°C for 40 min and the pellet was resuspended in buffer A containing 1% (w/v) *n*-dodecyl-β-D-maltoside (DDM). The suspension was centrifuged at 100,000 x *g* at 4°C for 40 min and then the supernatant which contains the overexpressed HubP truncation mutant was obtained.

3. Ligand-fishing experiment

3.1. Ligand fishing using metal affinity chromatography

V. vulnificus MO6-24/O cells grown overnight in LBS medium were harvested, washed, and resuspended in buffer B (50 mM sodium phosphate, pH 8.0, 200 mM KCl, and 5 mM imidazole). Cells were disrupted by three

passages through a French pressure cell at 8,000 psi, and centrifuged at 10,000 x *g* at 4ºC for 15 min. The supernatant was mixed with either buffer B as a control or purified His-tagged protein such as His-EIIA^{Glc} and His-FapA. EIIA^{Glc} was dephosphorylated by adding glucose or phosphorylated by incubating with PEP. Each mixture was then incubated with TALON metal affinity resin (Takara Bio) at 4ºC for 15 min. After three washes with buffer B, proteins bound to the column were eluted with 2x SDS loading buffer. The eluted protein samples (20 μl each) were analyzed by SDS-PAGE using a 4–20% gradient gel (KOMA BIOTECH) and staining with Coomassie brilliant blue R.

3.2. In gel-digestion

The protein bands of interest were excised from the gel which is stained with Coomassie brilliant blue R. The gel fragments were washed with isopropyl alcohol and deionized water. After equilibration with 200 mM ammonium bicarbonate, the gel fragments were dehydrated with 75% acetonitrile. The dehydrated gel fragments were dired in vacuum centrifuge, and then polypeptides in the gel fragments were digested by trypsin at a concentration of 10 ng/μl and incubated overnight. The digested peptides were extracted with 20 μl of 75% acetonitrile containing 5% trifluoroacetic acid and concentrated to about 5 μl in a vacuum centrifuge.

4. Confirmation of specific binding

4.1. Gel filtration chromatography of the protein-protein complex

4.1.1. Gel filtration chromatography of the EIIA^{Glc}-FapA complex

Gel filtration chromatography was carried out using an ÄKTA FPLC system (GE Healthcare Life Sciences). Each sample containing EIIA^{Glc} (97 μg), FapA (103 μg), or both proteins in 300 μl of buffer A was injected through a Superose 12 10/300 GL column (GE Healthcare Life Sciences) at

a flow rate of 0.5 ml min^{-1}. The three chromatograms were measured at 280 nm on the same scale, and then collected fractions (1 ml) were analyzed by SDS-PAGE using a 4–20% gradient gel (KOMA BIOTECH).

4.1.2. Gel filtration chromatography of the FapA-HubP complex

Gel filtration chromatography was carried out using an ÄKTA FPLC system (GE Healthcare Life Sciences). Each sample containing FapA (90 μg), HubP (165 μg), or both proteins in 300 μl of buffer A was injected through a Superose 6 10/300 GL column (GE Healthcare Life Sciences) at a flow rate of 0.5 ml min^{-1}. The three chromatograms were measured at 280 nm on the same scale, and then collected fractions (1 ml) were analyzed by SDS-PAGE using a 10% gel.

4.2. Surface plasmon resonance spectroscopy

Purified $EIIA^{Glc}$ was immobilized on the carboxymethylated dextran surface of a CM5 sensor chip by an NHS/EDC reaction, and real-time interaction of $EIIA^{Glc}$ with FapA was monitored by Surface Plasmon Resonance (SPR) detection using a BIAcore 3000 (GE Healthcare Life Sciences) as previously described (Lee et al. 2007; Park et al. 2013; Lee et al. 2014). The indicated concentrations of FapA in standard running buffer (10 mM HEPES, pH 7.5, 150 mM NaCl, 10 mM KCl, and 1 mM $MgCl_2$) were flowed over the $EIIA^{Glc}$ surface at a flow rate of 5 μl min^{-1}. The dissociation constant was calculated using BIAevaluation 2.1 software.

4.3. Native polyacrylamide gel electrophoresis

Native polyacrylamide gel electrophoresis was performed as described previously (Koo et al. 2004; Park et al. 2013). $EIIA^{Glc}$ (2.5 μg) and FapA (6 μg) were incubated at 37°C for 10 min in different combinations in 20 mM Tris-HCl buffer (pH 7.5) containing 2 mM $MgCl_2$, 10 mM KCl, 1 mM

dithiothreitol, and 2 mM PEP. To phosphorylate $EIIA^{Glc}$, EI and HPr (1 μg each) were added in the incubated reactions. Reaction mixtures were electrophoresed in a native 4–20% gradient gel (KOMA BIOTECH) and stained with Coomassie brilliant blue R.

5. Determination of the phosphorylation state of $EIIA^{Glc}$

Cell culture (0.2 ml at OD_{600} = 0.8) was quenched by mixing with 20 μl of 10 M NaOH, followed by vortexing for 10 s, and then 180 μl of 3 M sodium acetate (pH 5.2) and 1 ml of ethanol were added. Each sample was chilled at -70°C for 15 min, thawed and centrifuged at 4°C for 10 min. The pellet was rinsed with 1 ml of 70% ethanol, and resuspended in 50 μl of 2x SDS loading buffer. This solution (20 μl) was loaded onto a 4–20% gradient gel (KOMA BIOTECH). Proteins were transferred onto Immobilon-P membrane (EMD Millipore), immune-detected using a rat anti-$EIIA^{Glc}$ antiserum, and then visualized using Immobilon Western chemiluminescent HRP substrate (EMD Millipore) following the manufacturer's instructions.

6. Determination of cAMP concentration

Intracellular cAMP concentrations were measured as described previously (Colton et al. 2015) with some modifications. The amount of cAMP in the bacterial cell culture medium was estimated using the cAMP Biotrak enzyme immunoassay system according to the manufacturer's instructions (GE Healthcare Life Sciences). Cells were sampled at OD_{600} = 0.4 and 5 ml of culture were pelleted by centrifugation. The pellet was re-suspended in 540 μl of assay buffer and boiled 5 min. And then 60 μl of 2.5% dodecyltrimethylammonium bromide (Lysis reagent 1A) was added. The lysate was centrifuged at 10,000 x *g* at 4°C for 1 min, and the supernatant was used to determine the cAMP concentration.

7. Motility assay and transmission electron microscopy

V. vulnificus strains were grown to OD_{600} = 0.5 and spotted onto an LBS plate with 0.3% agar and 20 mM sodium phosphate (pH 8.0). The plate was incubated at 30ºC for 16 h. For transmission electron microscopy, cells grown to OD_{600} = 1.0 were harvested and resuspended in phosphate-buffered saline (PBS). Formvar-coated grid was immersed in the cell suspension, washed twice with sterile distilled water, and negatively stained with 2% uranyl acetate. Cells were monitored using a JEM1010 transmission electron microscope (JEOL).

8. Visualization of fluorescent fusion proteins in live cells

Cells were grown in LBS containing 0.02% L-arabinose to OD_{600} = 0.8, and spotted on a 1% agarose pad made with PBS on a glass slide. Cells were visualized using a Deltavision Restoration Microscope System (GE Healthcare Life Sciences).

9. RNA purification and qRT-PCR

Total RNA was isolated using an RNeasy minikit (Qiagen), and DNA was removed using an RNase-free DNase (Promega). For quantitative real-time PCR (qRT-PCR), cDNA was synthesized by cDNA EcoDry Premix (Takara Bio). Real-time PCR amplification of the 10-fold diluted cDNA was carried out using a CFX96 Real-Time System (Bio-Rad). Specific primers for amplification of the cDNA are listed in Table 2. To normalize the transcript level, 16S rRNA expression level was used as a reference.

10. 5' Rapid amplification of cDNA ends

The transcription start site of the *fapA* gene was determined using the 5' RACE System for Rapid Amplification of cDNA Ends, Version 2.0 (Thermo

Fisher Scientific Inc) following the manufacturer's instructions. cDNA was synthesized using a 5'-RACE P_1 primer, and a homopolymeric tail is added to the 3'-end of the cDNA using TdT and dCTP (included in the kit). 5'-RACE product was amplified by PCR from the dC-tailed cDNA using the abridged anchor primer (included in the kit) and 5' RACE P_2 primer, and then identified by sequencing. The gene specific reverse primers (5'-RACE P_1, P_2) are described in Table 2.

11. Comparison of virulence

Seven week old female ICR mice were used. Freshly cultured bacterial strains were washed and resuspended in PBS at a density of 1.5 X 10^5 cells/ml. Prior to bacterial inoculation, iron dextran (2 mg per mouse) was intraperitoneally injected into mice. After 30 min, 100 μl of bacterial suspensions or PBS were injected intraperitoneally into 10 mice. The number of dead mice was surveyed for 29 hours.

12. Isolation of flagellar hook basal body

Isolation of the flagellar basal bodies was performed as described previously (Terashima et al. 2006) with several modifications. Cells grown in LBS to OD_{600} = 1.0 were harvested, washed, and resuspended in sucrose buffer (50 mM Tris-HCl, pH 7.5, 0.5 M Sucrose). The suspension was converted into spheroplasts by adding lysozyme and EDTA to final concentrations of 0.1 mg ml^{-1} and 5 mM, respectively. The spheroplasts were lysed by adding Triton X-100 to a final concentration of 1% (w/v) and incubated for 1 h. To reduce the viscosity of the lysed spheroplasts, $MgSO_4$ and DNase I were added to final concentrations of 10 mM and 0.1 mg ml^{-1}, respectively, incubated at 30°C, and essentially completed in 30 min. Unlysed cells and cellular debris were removed by centrifugation at 12,000 g at 4°C for 20 min, and polyethylene glycol 8000 and NaCl were added to

the lysate to final concentrations of 2% and 100 mM, respectively. The suspension was incubated at 4°C for 1 h, and then centrifuged at 27,000 g at 4°C for 30 min. The pellet was resuspended in 6 ml of TED buffer (10 mM Tris-HCl, pH 8.0, 5 mM EDTA, 0.1% (w/v) DDM). The suspension was centrifuged at 1,000 g at 4°C for 15 min to remove cellular debris. The supernatant was centrifuged 100,000 g at 4°C for 30 min, and the pellet was resuspended in 200 μl of TED buffer. To dissociate the flagellar filaments into monomeric flagellin, the suspension was diluted 30-fold in 50 mM glycine-HCl, pH 3.5 containing 0.1% (w/v) DDM and shaken at 30°C for 60 min. After the sample was centrifuged at 1,000 g at 4°C for 15 min, the supernatant is centrifuged at 150,000 g at 4°C for 40 min. The pellet was resuspended in 100 μl of TED buffer.

Chapter III. Result

1. Flagellar motility in *V. vulnificus* is repressed in the presence of glucose.

1.1. Effect of glucose on motility and flagellar formation

To determine whether glucose functions as an attractant or inhibits flagellar motility in *V. vulnificus*, the effects of glucose on flagellar motility were measured. Approximately 10^6 wild-type cells were spotted on an LBS plate containing 0.3% agar, and then filter paper disks impregnated with glucose, mannitol, galactose, or glycerol were placed onto the plate at the same distance from the spot of cells. *V. vulnificus* cells migrated considerably faster toward glucose than toward other sugars (Figure 2A). Although comparison of swimming distances indicates that glucose is the most effective attractant of the tested sugars, swimming motility of *V. vulnificus* was suppressed by glucose when cells were incubated on a swimming plate supplemented with glucose, but not by other sugars (Figure 2B). It should be noted that an increase in cell density on the plate containing glucose indicates the growth of cells without moving outward from the inoculation point. Transmission electron microscopy analysis revealed that 87% of the cells grown in the presence of glucose had no flagella and the rest 13% of the cells had a short fragmented flagellum (Figure 3A and B). On the contrary, most cells synthesized a full-length flagellum in the absence of glucose, regardless of the presence of other sugars.

1.2. Effects of various PTS sugars on motility and flagellar formation

In order to deduce the regulator mediating the glucose-dependent prevention of flagellar synthesis, the effect of another PTS sugar on flagellar motility was examined. In *V. vulnificus*, the mannitol-specific EII shares EI and HPr with the glucose-specific EII for sugar transport and phosphorylation (Deutscher et al. 2014). Interestingly, unlike glucose,

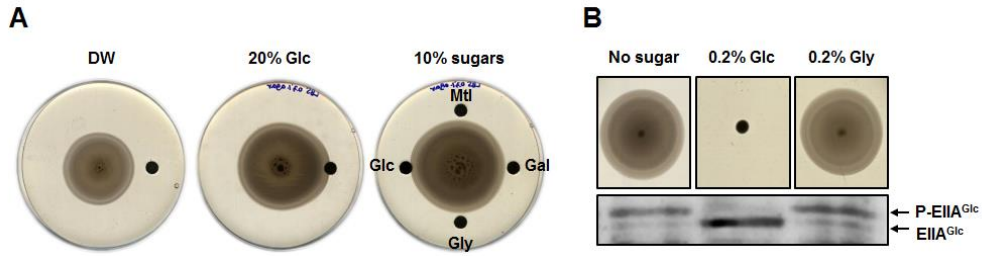

Figure 2. Effect of glucose on motility.

(A) Swimming motility of wild-type *V. vulnificus* cells toward attractants. Filter paper disks impregnated with distilled water (DW), glucose (Glc), mannitol (Mtl), galactose (Gal) or glycerol (Gly) were placed at 25-mm distance from the center as indicated. Cells were then spotted on the centers of 0.3% agar LBS plates, and incubated at 30°C for 16 h. (B) Effect of sugars on swimming motility of wild-type *V. vulnificus* cells. Cells were inoculated on a 0.3% agar LBS plate supplemented with glucose (Glc) or glycerol (Gly) (top panel). The phosphorylation state of $EIIA^{Glc}$ in each condition was examined using polyclonal antibodies against *V. vulnificus* $EIIA^{Glc}$ raised in rat (bottom panel).

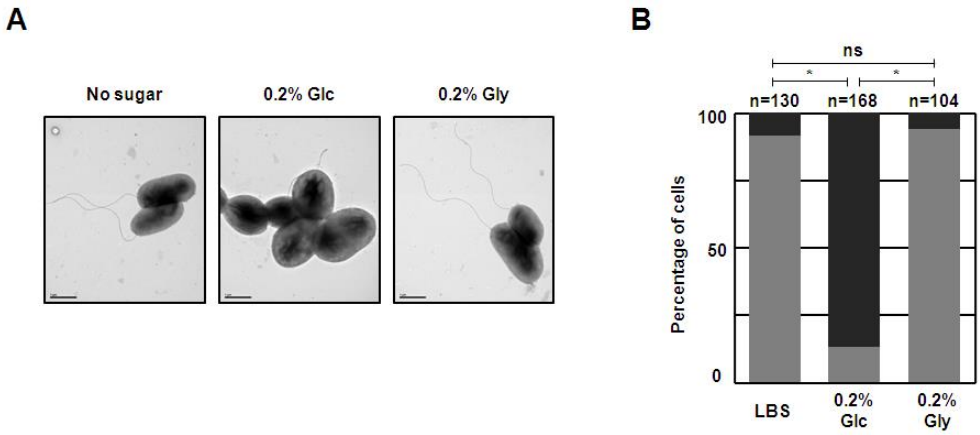

Figure 3. Effect of glucose on flagellar formation.

A. Electron micrographs of wild-type *V. vulnificus* cells grown in LBS supplemented with the indicated sugars. Cells were negatively stained with 2% (w/v) uranyl acetate. Bars, 1 μm.

B. The proportions of cells with (gray bars) or without (black bars) flagella in (A).

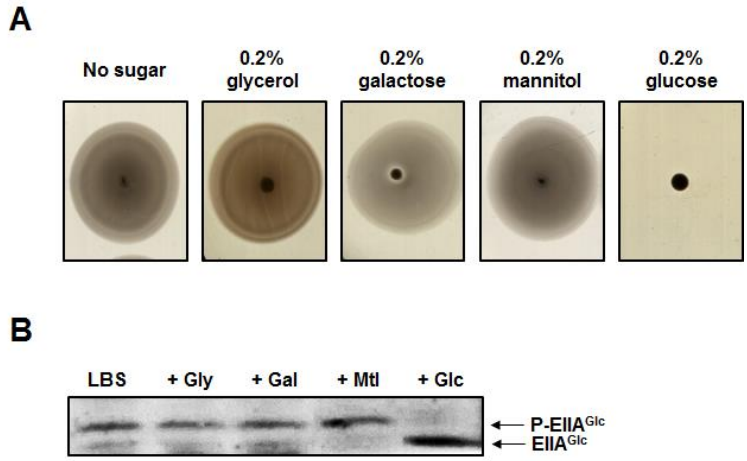

Figure 4. Effects of various sugars on motility.

A. Swimming motility of wild-type strains inoculated on a 0.3% agar LBS plate supplemented with indicated sugars. Plates were incubated at 30°C for 16 h.

B. Effect of various sugars on the phosphorylation state of $EIIA^{Glc}$. The phosphorylation state of $EIIA^{Glc}$ was examined using polyclonal antibodies against *V. vulnificus* $EIIA^{Glc}$ raised in rat. Cells (~$4x10^8$) grown to exponential phase in LBS or LBS supplemented with the indicated sugar were quenched to fix the phosphorylation state of $EIIA^{Glc}$, and Western blot analysis was performed as described in "Materials and Methods." Gly, glycerol; Gal, galactose; Mtl, mannitol; Glc, glucose.

mannitol did not suppress swimming motility of *V. vulnificus* (Figure 4). This result suggests that the regulator mediating the glucose-dependent prevention of swimming motility can be a component of glucose-specific EII, but not the general PTS proteins EI and HPr.

1.3. Genetic organization of chemotaxis gene clusters and the *pts* operon

The complete genome sequence of *V. vulnificus* MO6-24/O (Park et al. 2011) revealed several chromosomal loci with clusters of flagellar genes together with chemotaxis genes, as in *V. cholerae and V. parahaemolyticus* (Heidelberg et al. 2000; McCarter 2001; Boin et al. 2004). Notably, the *ptsHIcrr* operon encoding HPr, EI, and $EIIA^{Glc}$, respectively, is located next, albeit in the opposite orientation, to the flagellar gene cluster II (Figure 5). The bacterial PTS not only catalyzes sugar uptake and phosphorylation, but also is involved in multiple physiological regulations through protein-protein interactions in *E. coli* (Nam et al. 2001; Koo et al. 2004; Barabote et al. 2005; Deutscher et al. 2006; Park et al. 2013; Deutscher et al. 2014; Leng et al. 2016). All these regulatory processes depend on the phosphorylation state of the involved components. Because genes located in the same cluster often function in the same physiological context, it was expected that the PTS might be related to regulation of flagellar motility in *V. vulnificus*.

2. Dephosphorylated $EIIA^{Glc}$ inhibits flagellar motility in *V. vulnificus* by a cAMP-independent mechanism.

2.1. Inhibition of motility by dephosphorylated $EIIA^{Glc}$

In *E. coli*, $EIIA^{Glc}$ plays pivotal roles in the glucose-mediated regulation of carbon metabolism such as catabolite repression and senses glucose through its phosphorylation states (Deutscher et al. 2014). In *V. vulnificus*,

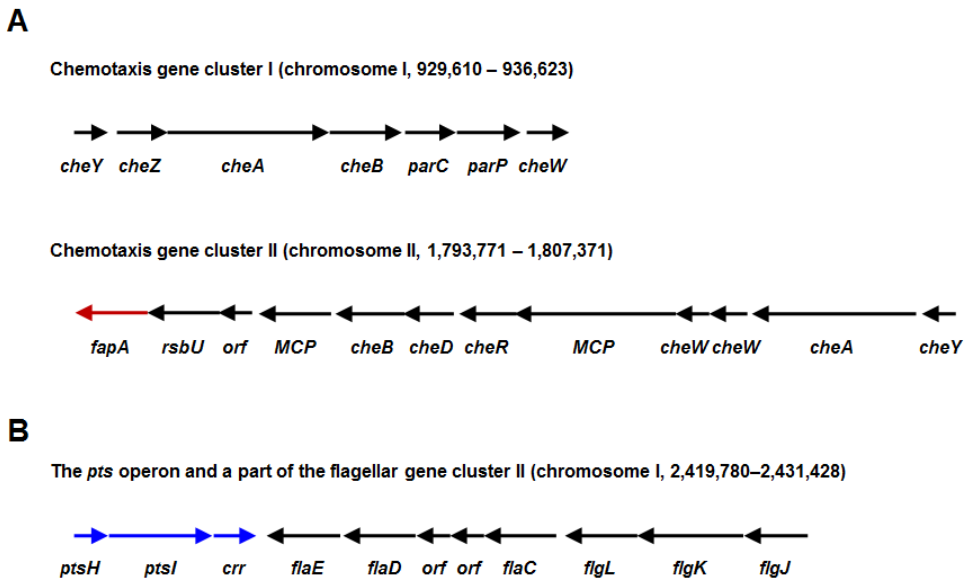

Figure 5. Genetic organization of two chemotaxis gene clusters and the *pts* operon in *V. vulnificus*.

A. Graphical depiction of the chemotaxis gene clusters I and II of *V. vulnificus*. Arrows denote ORFs with corresponding gene names below. The chemotaxis gene clusters I and II are located on chromosome I and II, respectively. The *fapA* gene (red arrow) is located at the end of the chemotaxis gene cluster II.

B. The location of the *ptsHIcrr* operon (blue arrows) next to the flagellar gene cluster II in the opposite direction on chromosome I.

the phosphorylation state of $EIIA^{Glc}$ was also changed depending on the availability of glucose and it exists mostly in a dephosphorylated form in the presence of glucose (bottom panel in Figure 2B and Figure 4B). To examined whether $EIIA^{Glc}$ plays a direct role in the regulation of swimming motility by sensing glucose, motility assay was performed. Unlike the wild-type strain, a *crr* mutant strain exhibited flagellar motility even in the presence of glucose (Figure 6A), implying that $EIIA^{Glc}$ negatively affects flagellar motility in the presence of glucose. To confirm whether dephosphorylated $EIIA^{Glc}$ inhibits flagellar motility, we constructed the pSY013 plasmid expressing a mutant form of $EIIA^{Glc}$(H91A) which cannot be phosphorylated by HPr. While the *crr* mutant strain harboring the wild-type $EIIA^{Glc}$ expression vector pSY012 exhibited swimming motility in LBS medium, the *crr* mutant strain harboring the pSY013 plasmid did not, even in the absence of glucose (Figure 6B). Therefore, these results indicate that $EIIA^{Glc}$ is dephosphorylated in the presence of glucose and this dephosphorylated $EIIA^{Glc}$ inhibits flagellar motility of *V. vulnificus*. This conclusion is supported by the fact that expression of $EIIA^{Glc}$(H91A) caused the entire loss of motility even in wild-type cells (Figure 7).

2.2. Effect of cAMP on the glucose-mediated inhibition of flagellar motility

It was hypothesized that the glucose dependent repression of flagellar motility might be explained by the lowered cAMP level as shown in some enteric bacteria such as *E. coli* (Yokota et al. 1970; Dobrogosz et al. 1971; Stella et al. 2008). Either the presence of glucose or the *crr* mutation significantly decreased the intracellular cAMP level (Figure 8A), as in *E. coli* (Levy et al. 1990; Nam et al. 2005). Intriguingly, however, the glucose effect on flagellar motility of *V. vulnificus* was certainly not due to a decrease in the cellular cAMP level since the addition of cAMP to the

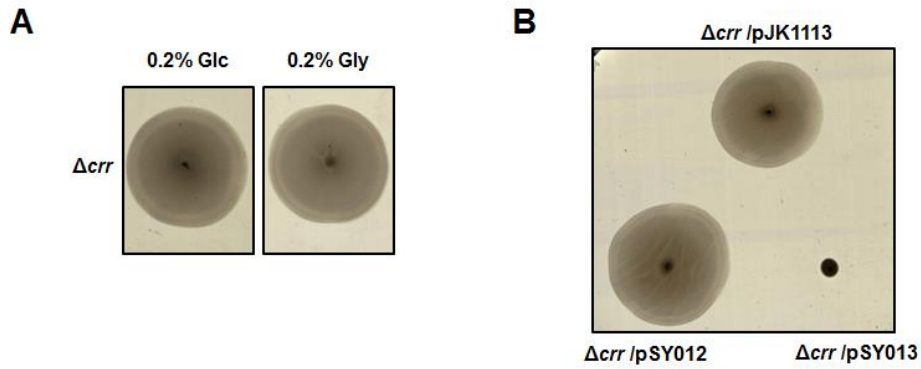

Figure 6. Inhibition of motility by dephosphorylated EIIA^{Glc}.

A. Swimming motility of *crr* mutant cells inoculated on a 0.3% agar LBS plate supplemented with glucose (Glc) or glycerol (Gly).

B. Swimming motility of *crr* mutant cells harboring the control vector pJK1113, pSY012 expressing wild-type EIIA^{Glc}, or pSY013 expressing EIIA^{Glc}(H91A) on 0.3% agar LBS plate without sugar. Plates were incubated at 30^{o}C for 16 h.

Figure 7. Inhibition of wild-type *V. vulnificus* motility by dephosphorylated EIIA^{Glc}.

The wild-type cells harboring the control vector pRK415 or the pRK415-based vector pSY011 expressing an unphosphorylatable form of EIIA^{Glc} were inoculated on a 0.3% agar LBS plate. The plate was incubated at 30ºC for 16 h.

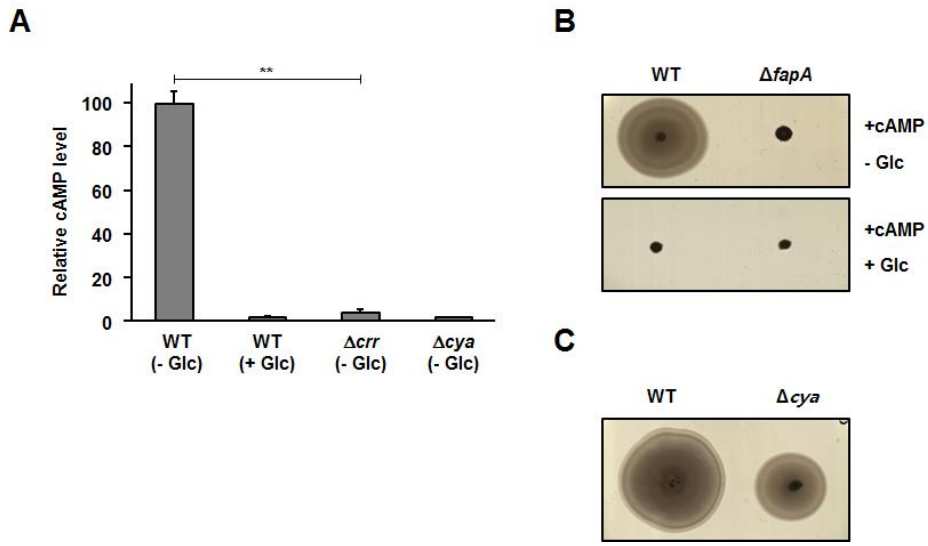

Figure 8. Effect of cAMP on the glucose-dependent repression of flagellar motility in *V. vulnificus*.

A. Relative levels of cAMP in wild-type, *crr* mutant, and *cya* mutnat strains grown in LBS with or without glucose as indicated. Error bars denote standard deviations from five measurements. Statistical significance was assessed using Student's *t*-test (**$p < 0.001$).

B. Swimming motility of wild-type and *fapA* mutant strains inoculated on the surface of a semi-solid LBS plate supplemented with 2.5 mM cAMP. Top panel: in the absence of glucose; bottom panel: in the presence of 1% (w/v) glucose (Glc).

C. Analysis of swimming motility of wild-type and *cya* mutant strains. Strains were inoculated on a 0.3% agar LBS plate and incubated at 30°C for 16 h.

culture medium did not relieve the inhibition of flagellar motility by glucose (Figure 8B). Moreover, a *cya* deletion mutant accumulating little cAMP retained the flagellar motility, even though this mutant had slower motility compared with the wild-type strain (Figure 8C). Preservation of the flagellar motility in the *V. vulnificus cya* mutant is in accordance with a previous report (Kim et al. 2005). These data together support that dephosphorylated $EIIA^{Glc}$ inhibits flagellar motility of *V. vulnificus* by a cAMP-independent mechanism.

3. Dephosphorylated $EIIA^{Glc}$ directly interacts with a flagellar assembly protein, FapA.

3.1. Ligand fishing using $EIIA^{Glc}$ as bait

To search for a regulator of flagellar motility operating downstream of and controlled by the phosphorylation state of $EIIA^{Glc}$, protein ligand fishing experiment was performed both in the presence and absence of glucose. Purified His-$EIIA^{Glc}$ was mixed with crude extracts of *V. vulnificus*, and these mixtures were incubated with either glucose to dephosphorylate or PEP to phosphorylate $EIIA^{Glc}$. Through several independent experiments, it was founded that a protein band migrating at approximately 100 kDa which was enriched in eluates containing His-$EIIA^{Glc}$ regardless of the phosphorylation state of $EIIA^{Glc}$ and two bands at approximately 60 and 45 kDa that were exclusively detected in the eluate containing dephosphorylated His-$EIIA^{Glc}$ (Figure 9). MALDI-TOF mass spectrometry and peptide mass fingerprinting revealed that the protein band migrating at 100 kDa corresponded to vIDE, which is already known to interact with $EIIA^{Glc}$ regardless of the phosphorylation state in *V. vulnificus* (Kim et al. 2010), while the band at 45 kDa was identified as the fermentation/ respiration switch protein FrsA, which only interacts with dephosphorylated $EIIA^{Glc}$ in *E. coli* and *V. vulnificus* (Koo et al. 2004; Lee et al. 2011).

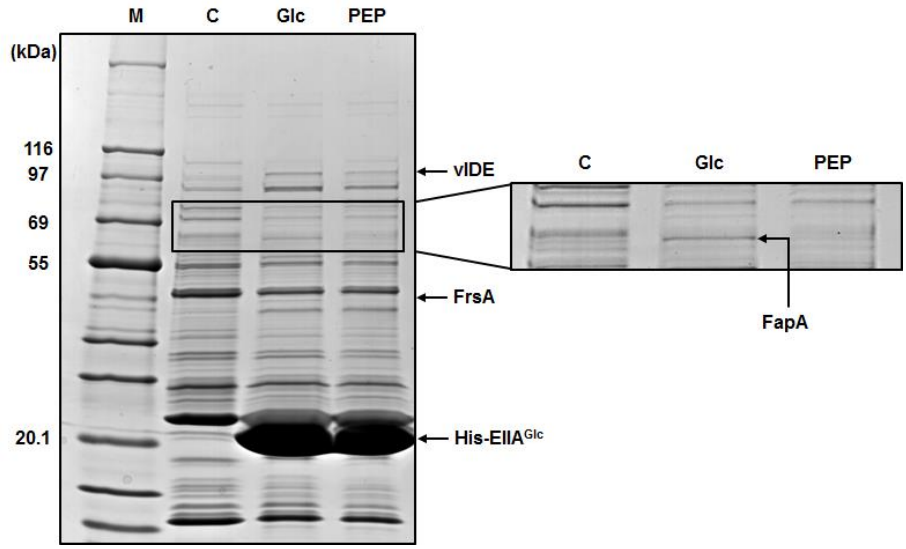

Figure 9. Ligand-fishing experiment to search for proteins interacting with His-EIIA^{Glc}.

A crude extract of wild-type *V. vulnificus* cells was incubated with buffer B (lane C) or 0.5 mg of purified His-EIIA^{Glc}. The extract containing purified His-EIIA^{Glc} was supplemented with either 2 mM glucose to dephosphorylate EIIA^{Glc} (lane Glc) or 2 mM PEP to phosphorylate EIIA^{Glc} (lane PEP). Each mixture was subjected to TALON metal affinity chromatography and proteins bound to the column were analyzed by SDS-PAGE using a 4–20% gradient gel (KOMA BIOTECH) and stained with Coomassie brilliant blue R.

Notably, the protein band of approximately 60 kDa was identified as a hypothetical protein of 557 amino acids encoded by VVMO6_04547 (henceforth referred to as FapA for flagellar assembly protein). This protein shares no homology with other known functional domains or motifs, and, therefore, it is currently classified as DUF342. Interestingly, this protein is encoded at the end of the chemotaxis gene cluster II (Figure 5A) and highly conserved in the family *Vibrionaceae* (Table 3), but rare in other bacteria and not found in the family *Enterobacteriacea*, including *E. coli*.

3.2. Confirmation of interaction between $EIIA^{Glc}$ and FapA

3.2.1. Confirmation of interaction between $EIIA^{Glc}$ and FapA using TALON metal-affinity resin

To explore the specific interaction between FapA and $EIIA^{Glc}$, a cell-free extract of *E. coli* expressing *V. vulnificus* FapA was mixed with various amounts of purified *V. vulnificus* His-$EIIA^{Glc}$ and subjected to pull-down assays. The amount of the FapA protein bound to the column increased with increasing concentrations of His-$EIIA^{Glc}$ added to the column (Figure 10), confirming that $EIIA^{Glc}$ specifically interacts with FapA.

3.2.2. Determination of the binding stoichiometry between $EIIA^{Glc}$ and FapA using a gel filtration column

The tight interaction between FapA and $EIIA^{Glc}$ was confirmed by gel filtration chromatography. The elution profile of the complex from a Superose 12 gel filtration column (10 × 300 mm, GE Healthcare Life Sciences) was compared with those of the individual proteins. Purified FapA alone was eluted with a peak at 10.75 ml, corresponding to its monomeric form (60 kDa), while $EIIA^{Glc}$ alone was eluted with a peak at approximately 13 ml with very little absorbance at 280 nm (Figure 11A) (Koo et al. 2004). When a mixture of the two proteins was loaded onto the column, the elution

Table 3. Distribution of FapA homologs in γ-proteobacteria

Organism	Accession number	Identity (%)	Family
Vibrio vulnificus CMCP6	VV2_1157	99	*Vibrionaceae*
Vibrio vulnificus YJ016	VV_RS23470	99	*Vibrionaceae*
Vibrio parahaemolyticus RIMD 2210633	VPA1749	72	*Vibrionaceae*
Vibrio alginolyticus 40B	VMC_06350	72	*Vibrionaceae*
Vibrio anguillarum 775	VAA_01913	62	*Vibrionaceae*
Vibrio cholerae El Tor N16961	VCA1085	62	*Vibrionaceae*
Aliibrio fischeri ES114	VF_1495	43	*Vibrionaceae*
Photobacterium profundum SS9	PBPRB2019	35	*Vibrionaceae*
Shewanella loihica PV-4	Shew_3231	34	*Shewanellaceae*
Shewanella baltica OS195	Sbal195_0837	34	*Shewanellaceae*
Colwellia psychrerythraea 34H	CPS_3684	31	*Colweliaceae*
Aeromonas hydrophila ATCC7966	AHA_0483	29	*Aeromonadaceae*
Alteromonas sp. SN2	AMBT_10260	29	*Alteromonadaceae*
Pseudoalteromonas haloplanktis TAC125	PSHAa2113	29	*Pseudoalteromonadaceae*

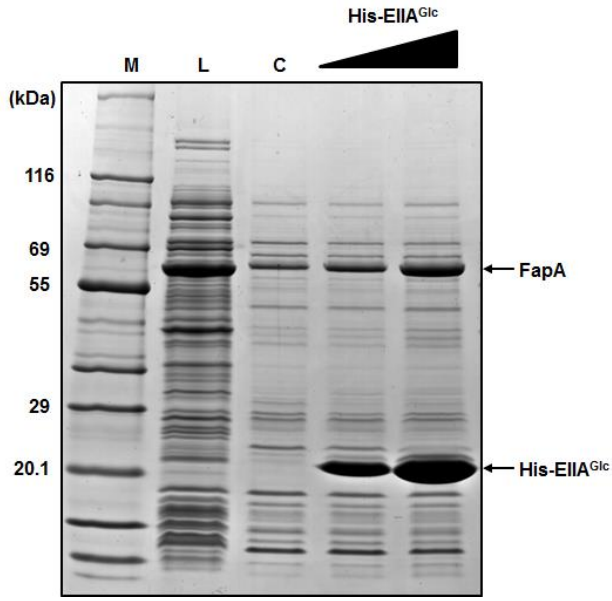

Figure 10. Specific interaction of FapA with EIIA^{Glc}.

An *E. coli* cell extract expressing FapA (5 mg protein) was mixed with various amounts (100 and 400 μg) of purified His-EIIA^{Glc} in a total volume of 250 μl. A cell extract without purified EIIA^{Glc} was used as a control. Each mixture was incubated with 50 μl of TALON metal-affinity resin (Takara Bio) in a column at 4^{o}C for 15 min. After the columns were washed with 5 volumes of the binding buffer (50 mM sodium phosphate, pH 8.0, 200 mM KCl and 5 mM imidazole), bound proteins were eluted with 60 μl of 2 x SDS loading buffer. Aliquots (20 μl) of the eluted samples were analyzed by SDS-PAGE and staining with Coomassie brilliant blue R: M, EzWay Protein Blue MW Marker (KOMA BIOTECH); L, 2 μl of the *E. coli* cell extract expressing FapA; C, control without adding His-EIIA^{Glc}.

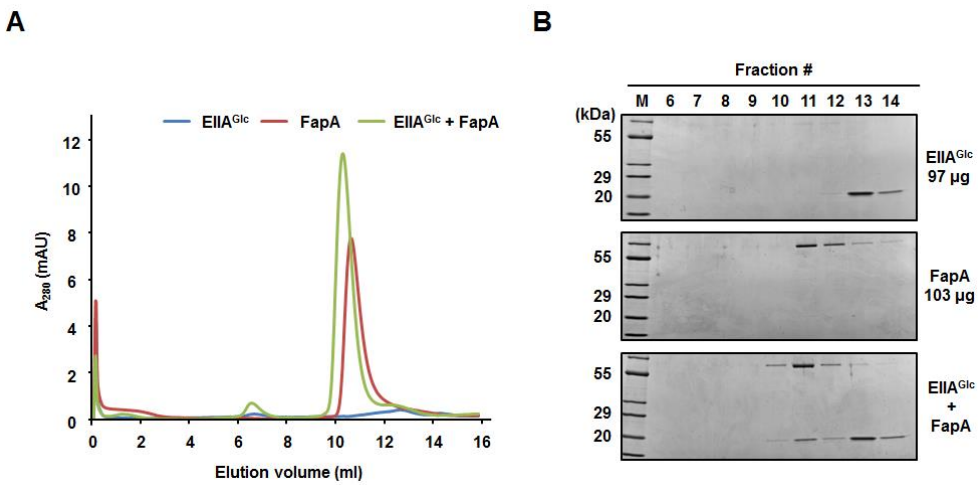

Figure 11. Gel filtration chromatography of EIIA^{Glc}, FapA and the EIIA^{Glc}-FapA complex.

A. Samples containing 97 µg of EIIA^{Glc}, 103 µg of FapA, or both proteins were injected through a Superose 12 10/300 GL column (GE Healthcare Life Sciences). Gel filtration was performed at a flow rate of 0.5 ml/min and the elution profiles were monitored by measuring the absorbance at 280 nm: blue line, EIIA^{Glc}; red line, FapA; green line, the EIIA^{Glc}-FapA mixture.

B. Fractions containing proteins were analyzed by SDS-PAGE.

peak shifted to approximately 10.39 ml. When the gel filtration fractions were analyzed by SDS-PAGE, those eluting at 10.39 ml were resolved into two bands of FapA and $EIIA^{Glc}$ (Figure 11B), indicating the tight interaction between FapA and $EIIA^{Glc}$. Based on the band intensities of the two proteins on SDS-PAGE of the corresponding fractions, it appears that $EIIA^{Glc}$ interacts with FapA in a 1:1 ratio to form a heterodimer.

3.2.3. Measurement of the dissociation constant between $EIIA^{Glc}$ and FapA using surface plasmon resonance spectroscopy

The binding constant between FapA and $EIIA^{Glc}$ was determined by surface plasmon resonance (SPR). $EIIA^{Glc}$ was immobilized on a CM5 sensor chip, and various concentrations of FapA were injected over the surface. Using the BIAevaluation 2.1 software, the dissociation constant (K_D) for the $EIIA^{Glc}$-FapA interaction was determined to be approximately 2.2×10^{-8} M, confirming the tight interaction between FapA and $EIIA^{Glc}$ (Figure 12).

3.2.4. Confirmation of interaction between dephosphorylated $EIIA^{Glc}$ and FapA using native polyacrylamide gel electrophoresis

In the ligand fishing experiment, FapA was detected only in the fraction mixed with dephosphorylated $EIIA^{Glc}$, but little, if any, in the fraction containing phosphorylated $EIIA^{Glc}$ (Figure 9). Because the regulatory functions of the PTS components generally depend on their phosphorylation state, I examined whether this interaction is dependent on the phosphorylation state of $EIIA^{Glc}$ by electrophoretic mobility shift assays on a nondenaturing polyacrylamide gel (Figure 13). When dephosphorylated $EIIA^{Glc}$ was run with FapA, the band intensity of $EIIA^{Glc}$ was significantly decreased with the concomitant appearance of a new band having higher band intensity and a slightly faster electrophoretic mobility than FapA

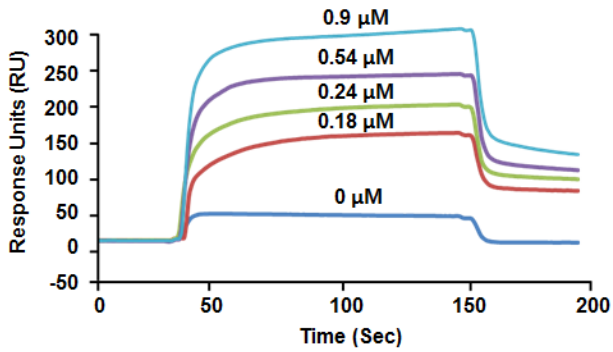

Figure 12. Measurement of the dissociation constant (K_D) between $EIIA^{Glc}$ and FapA.

Real-time interaction of $EIIA^{Glc}$ and FapA was monitored by surface plasmon resonance (SPR) detection using a BIAcore 3000 (GE Healthcare Life Sciences). Purified $EIIA^{Glc}$ was immobilized on a CM5 sensor chip, and various concentrations of FapA were injected over the surface. The K_D value between $EIIA^{Glc}$ and FapA was determined using BIAevaluation 2.1 software (GE Healthcare Life Sciences).

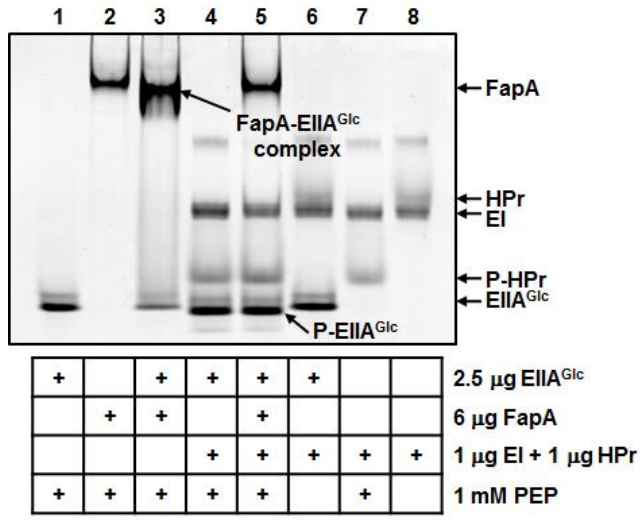

Figure 13. Specific interaction of FapA with dephosphorylated EIIA^{Glc}.
The specific interaction between dephosphorylated form of EIIA^{Glc} and FapA was determined by a native polyacrylamide gel electrophoresis. EIIA^{Glc} and FapA were incubated in different combinations in 20 mM Tris-HCl, pH 7.5, 2 mM $MgCl_2$, 10mM KCl, 1 mM dithiothreitol, and 2 mM PEP. Each reaction mixture was incubated at 37^{o}C for 10 min and then analyzed by native PAGE.

(compare lanes 1-3 in Figure 13). This result indicates that the FapA-EIIA^{Glc} interaction is strong enough to survive during PAGE under nondenaturing conditions as expected from the K_D value. When EIIA^{Glc} was reacted with PEP in the presence of EI and HPr, it could be completely phosphorylated as judged from the increased mobility of EIIA^{Glc} (lane 4 in Figure 13). Expectedly, the phosphorylated form of EIIA^{Glc} could not form the complex with FapA (compare lanes 4 and 5 in Figure 13). These results demonstrate that FapA specifically interacts with dephosphorylated EIIA^{Glc}.

4. Dephosphorylated EIIA^{Glc} inhibits flagellation by delocalizing FapA.

4.1. Phenotypes of the *fapA* mutant

To investigate the physiological role of FapA in *V. vulnificus*, phenotypes of an *fapA* mutant were compared with those of wild-type strain. While the *fapA* mutant showed little difference in growth compared to the wild type (Figure 14), this strain was non-motile regardless of the carbon source, and this loss of motility was turned out to be due to a complete failure of flagellar biosynthesis (Figure 15). Based on the complete loss of the flagellar assembly and motility in the *fapA* mutant, this hypothetical protein was named FapA (flagellar assembly protein A). It should be noted that flagellar motility could not be restored to the *fapA* mutant by the addition of cAMP (Figure 8B), indicating that FapA regulates flagellar biosynthesis by a cAMP-independent mechanism.

4.2. Localization of FapA to the flagellated pole

Members of the family *Vibrionaceae* display polarity as they assemble a single polar flagellum at the old pole (McCarter 2001) and the proteins involved in flagella formation are generally localized on the flagellated old cell pole (Kirkpatrick et al. 2011). For example, FlhF, the signal recognition

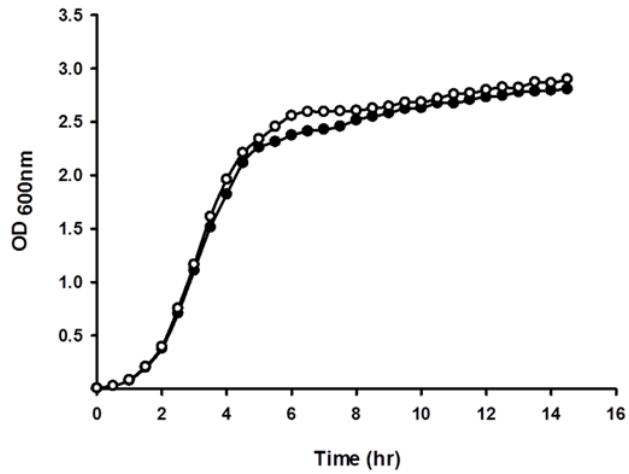

Figure 14. The growth curve of the *fapA* mutant.

V. vulnificus MO6-24/O (wild-type, closed circle) and the *fapA* mutant (open circle) were cultured in LBS. OD at 600 nm was measured every 20 minutes by bio-photorecorder® (Advantec®) at 30ºC.

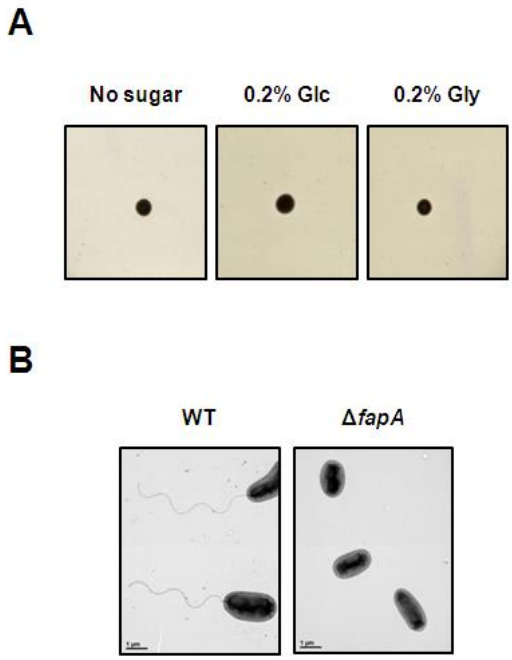

Figure 15. Swimming motility and flagella formation of the *fapA* mutant.

A. Swimming ability of an *fapA* mutant. Cells were inoculated on a 0.3% agar LBS plates supplemented with indicated sugars and incubated at 30°C for 16 h.

B. Electron micrographs of wild-type and *fapA* mutant cells. Cells were negatively stained with 2% (w/v) uranyl acetate. Bars, 1 μm.

particle (SRP)-type GTPase, is one of the determinants of the polar placement and assembly of the single flagellum. As previously shown (Kusumoto et al. 2008; Green et al. 2009), fluorescence microscopy revealed that the FlhF-green fluorescent protein fusion (FlhF-GFP) was localized at the flagellated pole in *V. alginolyticus* and *V. cholerae*. Based on the observation of flagellar deficiency in the *fapA* mutant, it was speculated that FapA might also be localized at the flagellated cell pole, where it helps flagellar assembly. To verify this assumption, green fluorescent protein (GFP) and red fluorescent protein (RFP) were fused to the N-terminus of FapA and the C-terminus of FlhF, respectively. GFP-FapA and FlhF-RFP were co-expressed in the wild-type cells, and their subcellular localizations were monitored by fluorescence microscopy (Figure 16). Most of the GFP-FapA foci were anchored at the cell pole and co-localized with the FlhF-RFP, suggesting that FapA is targeted to the flagellated pole in *V. vulnificus*.

4.3. Transcriptional activation of class III and IV flagellar genes by FapA

It has been shown that the flagellar biosynthesis regulator FlhF positively regulates the transcription of both class III and IV genes in the *Vibrionaceae* family members, whereas another flagellar biosynthesis regulator FlhG negatively regulates the transcription of all four classes of flagellar promoters (Correa et al. 2005; Kim et al. 2012). To determine whether FapA influences the transcription of flagellar genes, expression levels of several genes were measured by quantitative real-time PCR (qRT-PCR) analyses. Expression levels of class I (*flrA*) and class II (*fleS* and *flrC*) flagellar genes were not affected or slightly increased by the *fapA* mutation, whereas expression levels of the flagellar genes classified as class III (*fliD* and *flaC*) and class IV (*motX* and *flaFAG*) were decreased in the *fapA* mutant (Figure 17A). These results indicate that FapA positively regulates

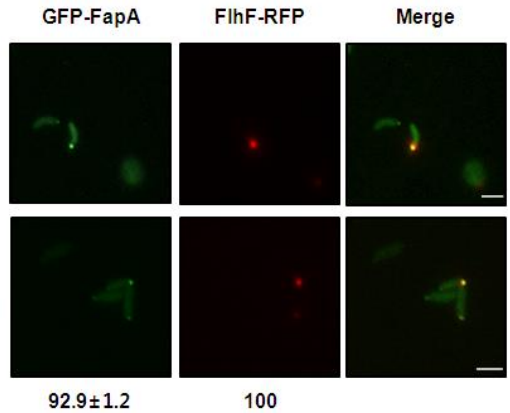

Figure 16. Co-localization of GFP-fused FapA (GFP-FapA) and RFP-fused FlhF (FlhF-RFP).

GFP-FapA and FlhF-RFP were co-expressed in a wild-type *V. vulnificus* strain and their subcellular localizations were monitored by fluorescence microscopy. The percentage of cells with polar foci in three independent experiments is shown at the bottom of each panel. Two representative fields are shown. Bars, 2 μm.

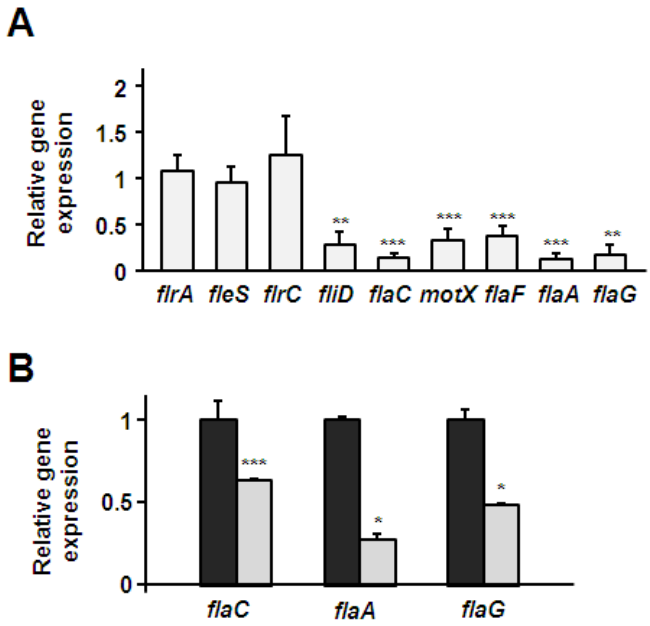

Figure 17. Determination of relative expression levels of indicated flagellar genes by qRT-PCR.

Each column represents the gene expression level in the *fapA* mutant relative to that in wild-type (A) or that in the wild-type cells harboring either pSY013 expressing EIIA^{Glc}(H91A) (light grey) relative to pJK1113-harboring cells (dark grey) (B). Average data from three independent experiments are shown. Asterisks indicate statistically significance assessed by the Student's *t*-test (*p< 0.05, **p< 0.01, ***p< 0.001).

the transcription of class III and IV flagellar genes and is functionally similar to the flagellar biosynthesis regulator FlhF.

4.4. Inhibiton of flagellar genes by dephosphorylated EIIA^{Glc}

To determine whether dephospho-EIIA^{Glc} can prevent the transcription of the flagellar genes through sequestration of FapA, the expression levels of class III and IV genes in wild-type strain harbouring the control plasmid pJK1113 or pSY013 expressing unphosphorylatable EIIA^{Glc}(H91A) were analyzed. The expression levels of the flagellar genes classified as class III (*flaC*) and class IV (*flaA* and *flaG*) were decreased in the strain overproducing EIIA^{Glc}(H91A) even in the absence of glucose (Figure 17B). This result indicates that EIIA^{Glc} prevents expression of the flagellar genes through sequestration of FapA in the presence of glucose. Because no DNA binding domain could be identified from the deduced amino acid sequence of FapA, further studies are required to elucidate the direct role of FapA in flagellar biosynthesis.

4.5. Delocalization of FapA from the pole by dephosphorylated EIIA^{Glc}

EIIA^{Glc} was predominantly phosphorylated in LBS medium supplemented with non-PTS carbon compounds or non-preferred PTS sugars, whereas it was almost completely dephosphorylated in LBS medium supplemented with glucose. Therefore, it was assumed that in the presence of glucose, dephosphorylated EIIA^{Glc} might inhibit flagellar motility of *V. vulnificus* by inhibiting the polar localization of FapA. In order to verify this assumption, I observed a cellular distribution of GFP-FapA in LBS medium supplemented with or without glucose. FapA was localized to the pole in LBS medium (Figure 18A). However, when glucose was added to LBS medium, the GFP-FapA foci almost completely disappeared from the pole and the protein was diffused throughout the cytoplasm. Notably, GFP-FapA

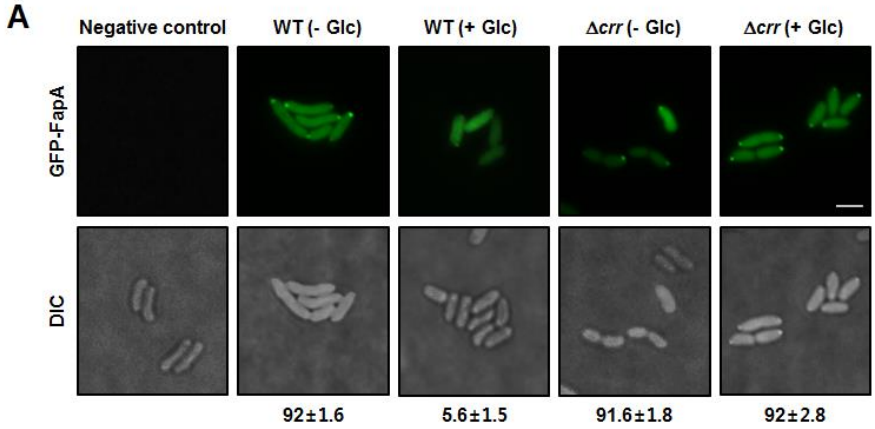
A
Negative control
WT (- Glc)
WT (+ Glc)
Δcrr (- Glc)
Δcrr (+ Glc)
GFP-FapA
DIC
92±1.6
5.6±1.5
91.6±1.8
92±2.8

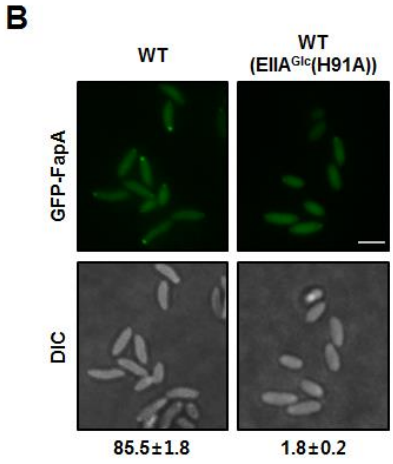
B
WT
WT
(EIIA^Glc(H91A))
GFP-FapA
DIC
85.5±1.8
1.8±0.2

Figure 18. Delocalization of FapA from the pole by dephosphorylated EIIA^{Glc}.

Fluorescence micrographs of GFP-FapA were obtained with indicated cells and phase micrographs of corresponding fields are shown in bottom panels. The percentage of cells with polar foci in three independent experiments is presented at the bottom of each panel. A representative field of each experiment was photographed. Bars, 2 μm.

A. Fluorescence micrographs of wild-type and *crr* mutant *V. vulnificus* cells harboring the pJK1113-based GFP-FapA expression vector pSY006 grown in LBS media with or without glucose in the presence of 0.02% (w/v) arabinose.

B. Effect of expression of dephosphorylated EIIA^{Glc} on polar localization of FapA. A *gfp-fapA* fusion gene and a mutated *crr* gene encoding EIIA^{Glc}(H91A) were cloned into a broad-host-range vector pRK415 and the pBAD-based expression vector pJK1113 to generate pSY014 and pSY013, respectively. The wild-type cells harboring pSY014 and either pJK1113 or pSY013 were grown in LBS medium in the presence of arabinose.

in the *crr* mutant was always localized to the pole regardless of the presence of glucose, whereas the episomal expression of unphosphorylatable $EIIA^{Glc}$(H91A) inhibited the polar localization of GFP-FapA even in the absence of glucose (Figure 18B). It should be noted that, while the addition of glucose completely delocalized FapA from the pole, the polar localization of FlhF was little affected by the presence of glucose in wild-type cells expressing both GFP-FapA and FlhF-RFP (Figure 19). Therefore, these results suggest that the polar localization of FapA is critical for the regulation of timely expression of flagellar genes and flagellar biosynthesis, and that dephosphorylated $EIIA^{Glc}$ delocalizes FapA from the flagellated pole through direct protein-protein interaction in the presence of glucose. However, it remains to be clarified how FapA regulates flagellar biosynthesis and the expression level of flagellar genes.

5. The *fapA* gene should be coordinately expressed with its upstream genes for flagellar motility.

5.1. Complementation of the *fapA* mutant by episomal expression of FapA

Because flagellar motility of a *V. vulnificus flhF* mutant could be restored to a wild-type level when FlhF was expressed from an arabinose-inducible plasmid in trans (Kim et al. 2012), I examined whether the episomal expression of *fapA* can also rescue the phenotype resulting from *fapA* mutation. Interestingly, the *fapA* mutant could not be complemented in trans by the arabinose-inducible FapA expression vector pSY015, which gave an approximately 9 times higher expression level of *fapA* than observed in the wild-type strain in the presence of arabinose (Figure 20A and B). Because the GFP-FapA fusion protein was localized to the cell pole in the absence of glucose and to the cytoplasm in the presence of glucose, it was examined whether the polar localization of GFP-FapA itself is enough

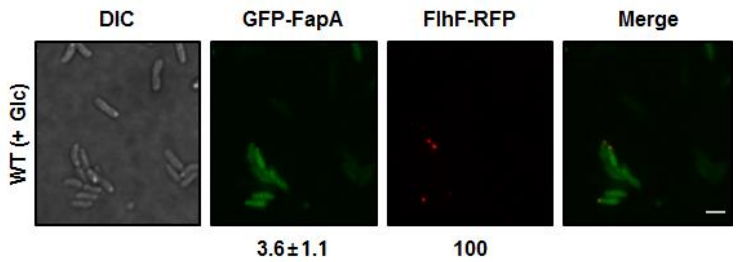

Figure 19. Effect of glucose on the polar localization of FapA and FlhF.
Wild-type cells harbouring pSY006 and the pJK1113-based FlhF-RFP expression vector pSY009 were grown in LBS medium supplemented with 0.5% (w/v) glucose and 0.02% (w/v) arabinose. Subcellular localization of GFP-FapA and FlhF-RFP were monitored by fluorescence microscopy. The percentage of cells with polar foci in three independent experiments is presented at the bottom of each panel. Bars, 2 μm.

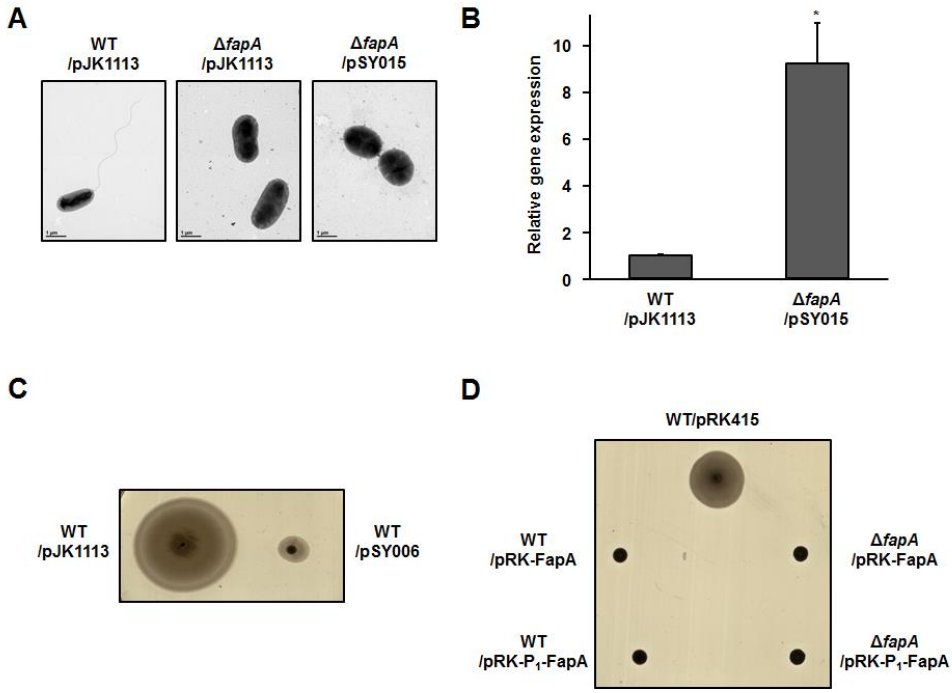
A
WT
/pJK1113
ΔfapA
/pJK1113
ΔfapA
/pSY015
B
Relative gene expression
0
2
4
6
8
10
*
WT
/pJK1113
ΔfapA
/pSY015
C
WT
/pJK1113
WT
/pSY006
D
WT/pRK415
WT
/pRK-FapA
ΔfapA
/pRK-FapA
WT
/pRK-P1-FapA
ΔfapA
/pRK-P1-FapA

Figure 20. Complementation of the *fapA* mutant by episomal expression of FapA.

A. Wild-type *V. vulnificus* cells harboring the control vector pJK1113 and the *fapA* mutant cells harboring either pJK113 or pSY015 expressing wild-type FapA were grown to exponential phase in LBS medium supplemented with 0.002% (w/v) L-arabinose and negatively stained with 2% (w/v) uranyl acetate, and then observed using a transmission electron microscope. Bars, 1 μm.

B. Determination of relative transcription levels of *fapA* gene by qRT-PCR. Error bars denote standard deviations from four measurements. Statistical significance was assessed using Student's *t*-test (*$p < 0.01$).

C. Wild-type cells harboring pJK1113 or pSY006 expressing GFP-FapA were inoculated on a 0.3% agar LBS plate supplemented with 0.2% L-arabinose and incubated at 30°C for 16 h.

D. Wild-type and *fapA* mutant strains expressing FapA from the *lac* promoter in pRK415 (pRK-FapA) or from the P_1 promoter upstream of the *fapA* gene (pRK-P_1-FapA) were inoculated on a 0.3% agar LBS plate and incubated at 30°C for 16 h to test swimming motility.

to render the cells motile. Interestingly, the wild-type *V. vulnificus* strain harboring the pJK1113-based GFP-FapA expression vector pSY006 lost its motility (Figure 20C). Moreover, out of wild-type and *fapA* mutant strains harboring the control vector pRK415 or pRK415-based FapA expression vector pRK-FapA, only the wild-type strain harboring the control vector retained the flagellar motility (Figure 20D). These data imply that FapA needs to be expressed in the right amount for flagellar motility in *V. vulnificus*.

5.2. Coordinate expression of *fapA* with its upstream genes

Because flagellar genes are known to be hierarchically expressed under strict control in *Vibrio* and *Pseudomonas* species (Correa et al. 2005; Moisi et al. 2009) and the *fapA* gene is located at the 3'-end of the chemotaxis gene cluster II (Figure 5), a 5'-RACE experiment was performed to find out whether this gene has its own promoter or it is co-transcribed with other genes as an operon. Consequently, it was identified that a transcription start site (TSS: P_1 in the Figure 21A) located at 377 bp upstream of the translation start codon of FapA within the ORF of the upstream gene VVMO6_04548. However, the expression level of *fapA* from this promoter, even on the multicopy plasmid pRK415, was significantly lower than observed in wild-type cells grown under the same condition (Figure 21B), implying the existence of another strong promoter located further upstream of P_1. Then, through RT-PCR analysis, it was found that the majority of *fapA* is indeed co-transcribed with at least four upstream genes as an operon in the chemotaxis gene cluster II (Figure 21C). Episomal expression of FapA to a lower level (about 28.6% of that observed in wild-type cells) from the pRK-P_1-FapA plasmid could not recover the flagellar biosynthesis and motility of the *V. vulnificus fapA* mutant (Figure 21D and E). Furthermore, transformation of the wild-type *V. vulnificus* strain with pRK-

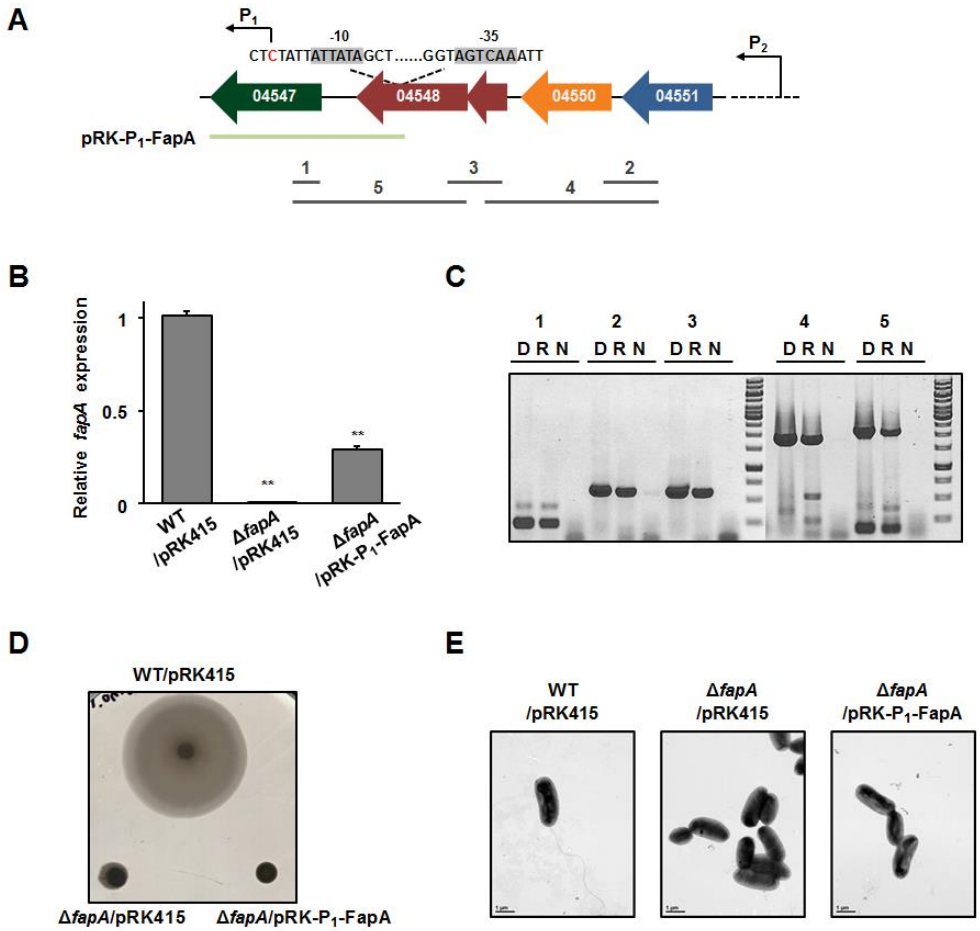

Figure 21. Coordinate expression of *fapA* with its upstream genes is required for flagellar synthesis.

A. Schematic representation of a part of the chemotaxis gene cluster II. Colored arrows indicate open reading frames and their direction of transcription. The ORF 04547 corresponds to the *fapA* gene encoded by VVMO6_04547. The P_1 promoter was identified at 377 bp upstream of the

translation start site of FapA by a 5'-RACE experiment. Characters shaded in grey indicate -10 and -35 regions of the promoter and the transcription start site is colored in red. The green bar represents the DNA fragment containing the *fapA* gene along with its P_1 promoter cloned into the broad-host-range vector pRK415 to generate pRK-P_1-FapA. Grey bars with numbers indicate reverse transcription (RT)-PCR products analyzed in (C).

B. Determination of the relative transcription level of the *fapA* gene in wild-type *V. vulnificus* strain harboring pRK415 and the *fapA* mutant strain harboring pRK415 or pRK-P_1-FapA plasmid by qRT-PCR. Error bars denote standard deviations from three measurements. Statistical significance was assessed using Student's *t*-test (**$p < 0.001$).

C. Analysis of co-transcription of *fapA* with its upstream genes by RT-PCR. RNAs from wild-type *V. vulnificus* cells were subjected to RT-PCR analysis using specific internal primers (see Table 2 for primers used for RT-PCR) within the chemotaxis gene cluster II as shown in (A). RT-PCR products were electrophoresed on a 1% agarose (lanes R), along with corresponding PCRs without reverse transcriptase (lanes N) and PCR products amplified using genomic DNA (lanes D) to demonstrate specificity of primers.

D. Swimming motility of the indicated strains on an LBS plate with 0.3% agar. The plate was incubated at 30^{o}C for 16 h.

E. The indicated strains were grown to exponential phase in LBS medium and negatively stained with 2% (w/v) uranyl acetate, and then subjected to transmission electron microscopy. Bars, 1 μm.

P_1-FapA also resulted in the loss of flagellar motility (Figure 20D). Therefore, these data suggest that FapA should be coordinately expressed with its upstream genes in the right amount for flagellar motility in *V. vulnificus*.

6. Effect of FapA on pathogenicity of *V. vulnificus*

V. vulnificus is an opportunistic human pathogen that is highly lethal and is responsible for the overwhelming majority of reported seafood-related deaths (Jones et al. 2009). Estuarine seawater, which is natural habitat for *V. vulnificus*, is oligotrophic and thus short of glucose. After infection to human, the bacterial cells might recognize the host environment by sensing chemicals such as glucose, which induces dephosphorylated $EIIA^{Glc}$ and thus inhibits FapA-mediated flagellation. This phenomenon may be involved in pathogenicity. To verify this hypothesis, a functional role of *V. vulnificus* FapA in mouse lethality was examined. 1.5 X 10^4 cells of wild-type or *fapA* mutant strains were injected intraperitoneally into seven-week-old female ICR mice with pretreatment with iron-dextran. All the mice injected with wild-type cells died within 23 h, whereas those injected with *fapA* mutant cells showed attenuation in mouse lethality (Figure 22). These results suggest that FapA is important for survival of this pathogen during host infection.

7. FapA specifically interacts with HubP.

7.1. Ligand fishing using FapA as bait

Dephosphorylated $EIIA^{Glc}$ inhibited flagellar motility by delocalization of FapA from the cell pole in *V. vulnificus*. However, it was still unclear how FapA specifically regulated the polar targeting and flagellar synthesis. To speculate the specific function and search for a new binding partner of FapA, ligand fishing experiment was performed using an N-terminally His_6-tagged

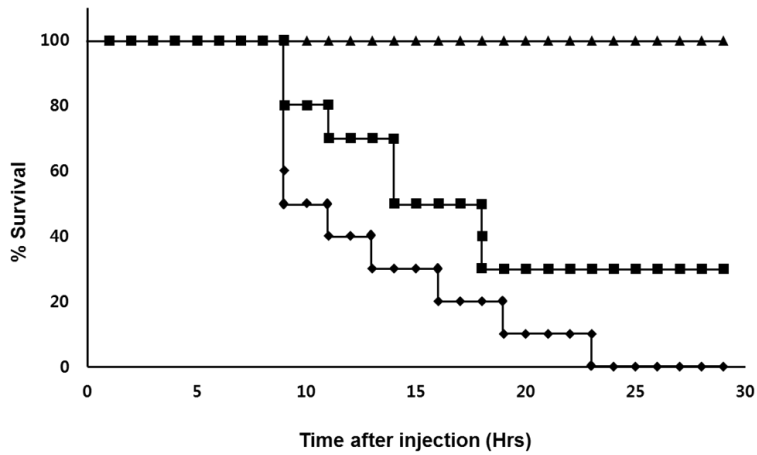

Figure 22. Effect of FapA on virulence in mice.

1.5 X 10^4 bacterial cells/mouse were injected to each 2 mg of iron dextran pre-treated 10 mice per strains, and during 29 hours the number of dead mice was counted. Diamond, mice injected with wild-type cells; square, mice injected with fapA mutant cells; triangle, mice injected with PBS.

form of FapA (His-FapA) as bait. Crude extracts prepared from wild-type *V. vulnificus* cells grown to stationary phase were mixed with purified His-FapA, and then incubated with either glucose to dephosphorylate or PEP to phosphorylate $EIIA^{Glc}$, since interaction with $EIIA^{Glc}$ and the regulatory functions of the FapA depends on the presence or absence of glucose. After these mixtures were subjected to pull-down assays, proteins bound to the resin were eluted with 2x SDS loading buffer. Analysis of the eluted proteins by SDS-PAGE followed by staining with Coomassie brilliant blue revealed that a protein band migrating at approximately 20 kDa was exclusively detected in the eluate containing glucose. Interestingly, a protein migrating approximately 220 kDa was always co-eluted with His-FapA (Figure 23). In-gel tryptic digestion, MALDI-TOF mass spectrometry, and peptide mass fingerprinting revealed that the protein band migrating at ~20kDa corresponded to $EIIA^{Glc}$, of which dephosphorylated form was already known to interact with FapA. The protein band at ~ 220kDa was identified as a HubP (hub of the pole) encoded by VVMO6_00873.

Several features of the HubP Protein in *V. vulnificus* were found by sequence and genomic analysis (Figure 24). HubP is a quite huge (~ 213kDa) transmembrane protein and its pI is approximately 3. Its N terminus consists of a signal peptide, a LysM domain which binds to peptidoglycan in *P. aeruginosa* (Semmler et al. 2000; Wehbi et al. 2011) and is required for polar localization in *V. cholera* and *S. putrefaciens* CN-32 (Yamaichi et al. 2012; Rossmann et al. 2015), and a single transmembrane spanning domain. Its C terminal cytoplasmic region is comprised of 5 copies of an imperfect 83-amino-acid repeat where 31 of the amino acids are acidic, i.e. glutamic acid and aspartic acid. It has been reported that the HubP is well conserved in *Vibrionaceae/Photobacteriaceae,* and has 48% and 45% of sequence identity with its orthologs in *V. cholerae* and *V. alginolyticus,* respectively.

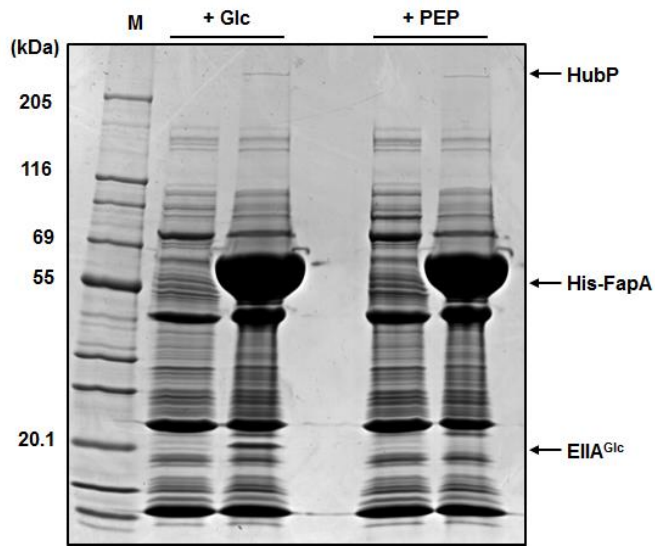

Figure 23. Ligand-fishing experiment to search for proteins interacting with His-FapA.

Purified His_6-tagged FapA (His-FapA) was mixed with *V. vulnificus* crude extract containing glucose (Glc) or PEP to control the phosphorylation state of $EIIA^{Glc}$. Each mixture was subjected to TALON metal affinity chromatography (Takara Bio) and proteins bound to the column were analyzed by SDS-PAGE using a 4-20% gradient gel (KOMA BIOTECH) and stained with Coomassie brilliant blue R.

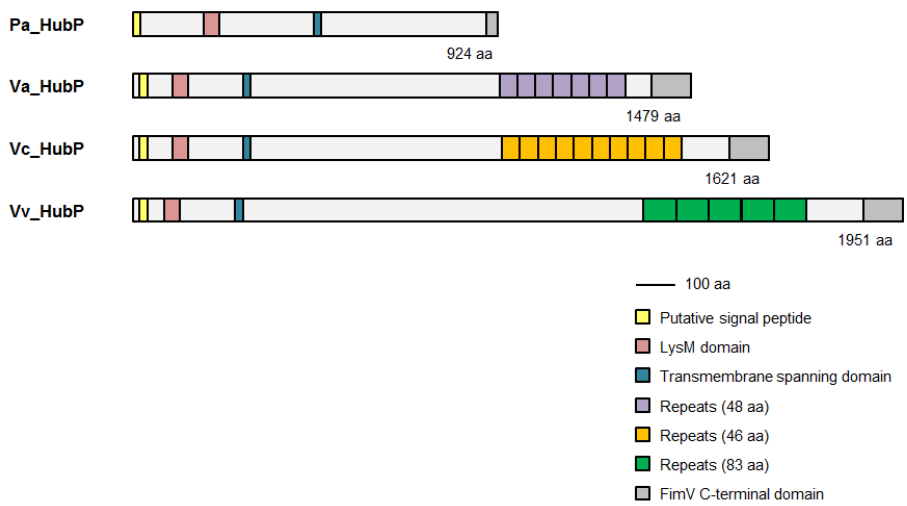

Figure 24. Schematics of HubP homologs.

Schematic presentation of several HubP homologs; *P. aeruginosa* FimV (Pa_HubP), *V. alginolyticus* HubP (Va_HubP), *V. cholerae* HubP (Vc_HubP) and *V. vulnificus* HubP (Vv_HubP).

7.2. Confirmation of interaction between FapA and HubP

7.2.1. Confirmation of interaction between FapA and HubP using ligand fishing experiment

To further confirm the specific interaction between FapA and HubP, ligand fishing experiment were performed using TALON metal affinity resin charged with His-FapA to identify interaction partners from crude extracts of wild-type *V. vulnificus* MO6-24/O and its isogenic *hubP* mutant cells. After brief washes and elution, a protein band migrating at ~213 kDa was only detected in the eluate from the column loaded with a mixture of the wild-type cells (Figure 25). Peptide mass fingerprinting after in-gel tryptic digestion identified this protein as HubP. This result supports a specific interaction between FapA and HubP.

7.2.2. Confirmation of interaction between FapA and HubP truncation mutant using TALON metal-affinity resin

Distinct cytoplasmic portions of HubP are required for binding and polar targeting of the partner proteins in *V. cholerae* (Yamaichi et al. 2012), implying that FapA might also interact with distinct region of HubP in *V. vulnificus*. To verify this assumption, series of HubP truncation mutants were expressed in *E. coli* cells (Figure 26). Crude extracts from soluble variants of HubP-expressed cells or detergent-solubilized membrane fraction from insoluble variants of HubP-expressed cells were mixed with the purified His-FapA bound TALON metal affinity resin, and subjected to pull-down assay. Unexpectedly, analysis of the eluted proteins by SDS-PAGE followed by staining with Coomassie brilliant blue R revealed that all the HubP truncated mutants were co-eluted with the His-FapA (Figure 27). It suggests that FapA interacts directly with random cytoplasmic portions of HubP.

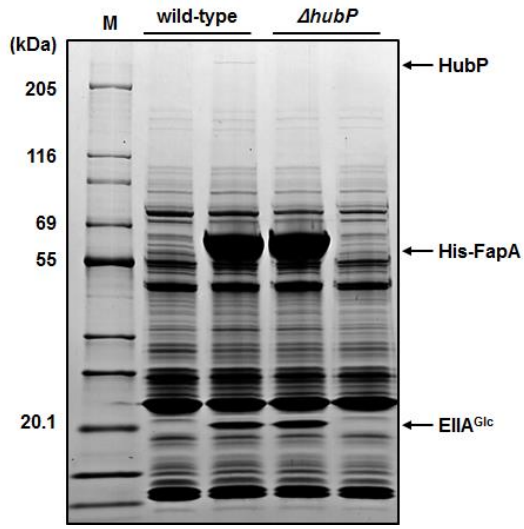

Figure 25. Specific interaction of FapA with HubP.

Ligand fishing experiment using His-FapA as baits. Crude extract from wild-type *V. vulnificus* or Δ*hubP V. vulnificus* grown in 200 ml of LBS was mixed with 350 μg of His-FapA or buffer B. These mixtures were incubated with 90 μl of TALON resin (Takara Bio) for metal affinity chromatography and analyzed by SDS-PAGE using a 4-20% gradient gel (KOMA BIOTECH). Protein bands bound specifically to His-tagged baits are indicated by arrows. M, EzWay Protein Blue MW Marker (KOMA BIOTECH).

Figure 26. Schematics of HubP truncation mutants.

Schematic presentation of the HubP polypeptide (top) and truncation mutants (bottom) used in this study. Yellow, Signal sequence; pink, LysM domain; blue-green, transmembrane domain; green, 5x repeats; gray, FimV C-terminal domain.

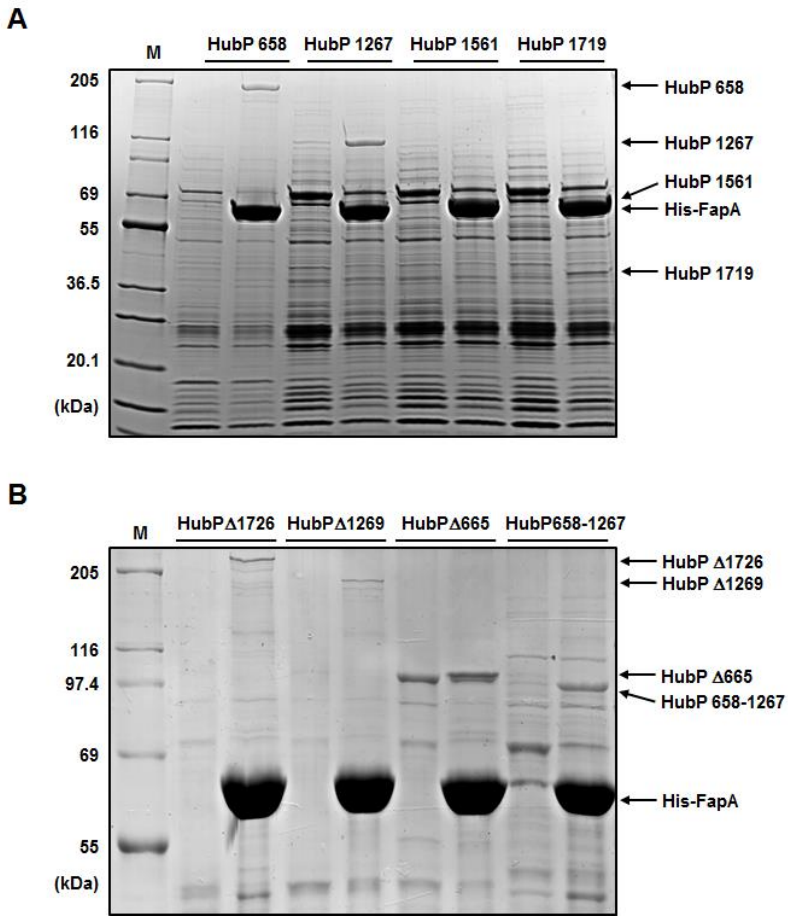

Figure 27. Specific interaction of FapA with HubP truncation mutants.
An *E. coli* cell extract expressing HubP truncation mutant was mixed with 100 μg of purified His-FapA in a total volume of 550 μl. A cell extract without purified His-FapA was used as a control. Each mixture was subjected to TALON metal affinity chromatography (Takara Bio) and proteins bound to the column were analyzed by SDS-PAGE using a 4-20% gradient (top, KOMA BIOTECH) and 10% gel (bottom), and stained with Coomassie brilliant blue R. M, EzWay Protein Blue MW Marker (KOMA BIOTECH).

It was previously demonstrated that high staining intensity by Coomassie R is related with interaction between Coomassie R ligands and protein molecules (Wilson 1979). Especially, the number of positive charged amino acids of the protein molecules, such as Lys, His, and Arg residues, is important for their interaction (Tal et al. 1985). It was also reported that high content of acidic amino acids in a protein shows slower electrophoretic mobility in SDS-PAGE (Guan et al. 2015). HubP is comprised of 3.3 and 32.5 percentages of basic and acidic amino acids (65 of basic and 634 of acidic amino acids in total 1951 of amino acids), respectively. In these reasons, HubP and its truncation mutants showed low Coomassie brilliant blue R staining intensity and larger than estimated size in the SDS-PAGE analysis.

7.2.3. Confirmation of interaction between FapA and HubP truncation mutant using a gel filtration column

The tight interaction between HubP 1267 and FapA was confirmed by gel filtration chromatography. The elution profile of the complex from a Superose 6 gel filtration column (10 × 300 mm, GE Healthcare Life Science) was compared with those of the individual proteins. Purified HubP 1267 alone was eluted with a peak at 9.28 ml whereas FapA was eluted at 14.36 ml (Figure 28A). When a mixture of the two proteins was subjected to the gel filtration chromatography, the HubP 1267 peak was increased with a concomitant disappearance of the FapA peak. When the gel filtration fractions were analyzed by SDS-PAGE, those eluting at 9.28 mL were resolved into two bands for HubP 1267 and FapA, indicating the tight interaction between two proteins (Figure 28B). However, I have been unable to determine the stoichiometry of HubP 1267-FapA interaction using the band intensities of each protein on SDS-PAGE of the corresponding fractions.

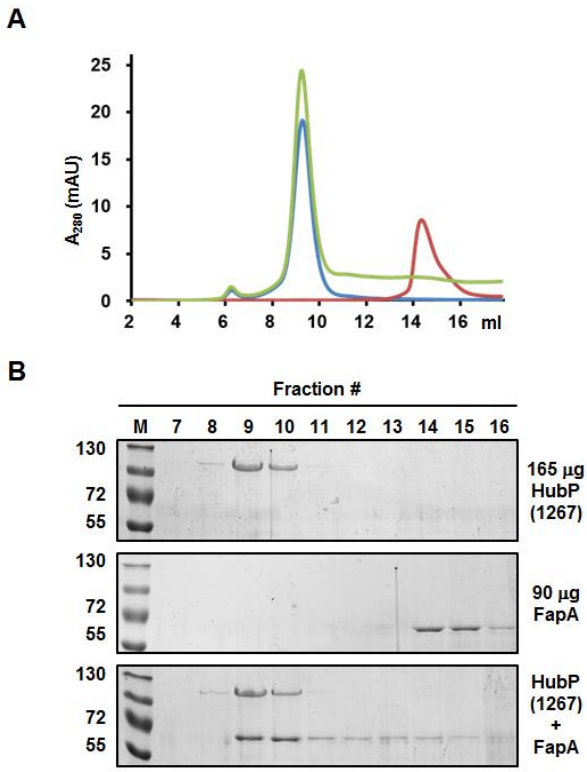

Figure 28. Gel filtration chromatography of HubP 1267, FapA and the HubP 1267-FapA complex.

A. Samples containing 165 µg of HubP 1267, 90 µg of FapA, or both proteins were injected through a Superose 6 10/300 GL column (GE Healthcare Life Sciences). Gel filtration was performed at a flow rate of 0.5 ml/min and the elution profiles were monitored by measuring the absorbance at 280 nm: blue line, HubP 1267; red line, FapA; green line, the HubP 1267-FapA mixture.

B. Fractions containing proteins were analyzed by SDS-PAGE using 10% gel. M, PageRuler™ Plus Prestained Protein Ladder (ThermoFisher Scientific).

8. HubP binds directly to FapA to control its subcellular distribution.

8.1. HubP, a determinant of polar FapA localization

Given the specific interaction of FapA with HubP, I assessed whether HubP is needed to localize the FapA. Before verification of this experiment, firstly, I observed whether HubP itself is present at the *V. vulnificus* cell poles. Red fluorescent protein (RFP) fused HubP (HubP-RFP) were ectopically expressed in a strain with an in-frame deletion of *hubP* and visualized by fluorescence microscopy. Expectedly, the fusion proteins were mainly detectable at the cell pole (Figure 29A). In wild-type cells, N-terminally green fluorescent protein (GFP) fused FapA (GFP-FapA) were polar localized at either one or both poles, as previously shown (Figure 16, 18 and 29B). However, the distribution of FapA was different in strains lacking *hubP*. GFP-FapA foci disappeared from the cell poles, and the proteins were diffused throughout the cell (Figure 29B). Furthermore, this pattern was restored in the *hubP* deletion strain by expression of the wild-type HubP in *trans*. When GFP-FapA and HubP-RFP were co-expressed in the Δ*hubP* strain, most of the GFP-FapA were positioned at cell poles and co-localized with HubP-RFP (Figure 30A). Together, these observations suggest that HubP is a determinant of polar FapA targeting through direct protein-protein interaction.

It has been reported that the N-terminal periplasmic LysM domain of HubP is required for its polar targeting in *V. cholerae* and *S. putrefaciens CN-32* (Yamaichi et al. 2012; Rossmann et al. 2015). To determine whether the N-terminal domain of HubP is important for the polar localization of HubP and hence FapA in *V. vulnificus*, HubP 658-RFP and GFP-FapA were co-expressed in a *hubP* deletion strain (Figure 30B). Expectedly, most of the GFP-FapA foci failed to restore polar placement, providing evidence that HubP association with the poles through its LysM domain is required for polar FapA localization.

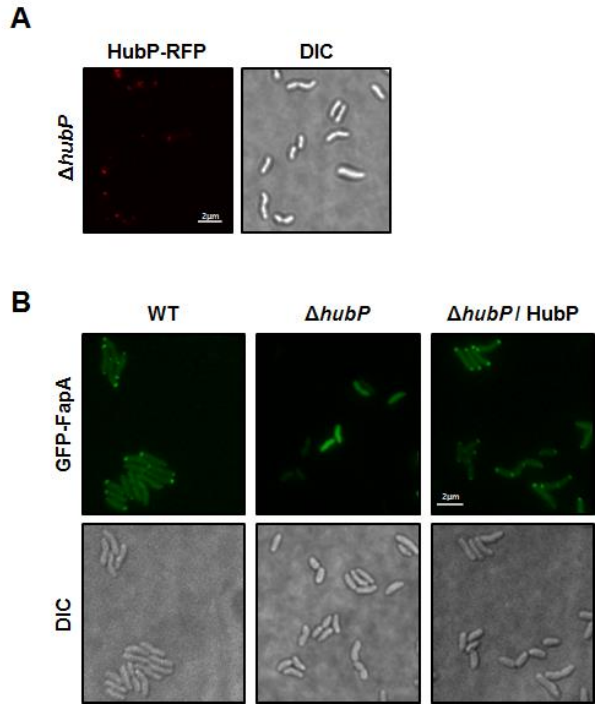

Figure 29. Subcellular localization of RFP-fused HubP (HubP-RFP) or GFP-fused FapA (GFP-FapA) in the indicated *V. vulnificus* strains.

A. RFP-fused HubP (HubP-RFP) in Δ*hubP V. vulnificus*, and its subcellular localization was monitored by fluorescence microscopy.

B. GFP-fused FapA (GFP-FapA) was expressed in the indicated *V. vulnificus* strains, and its subcellular localization was monitored by fluorescence microscopy.

Pictures shown are representative fields. Bars, 2 μm.

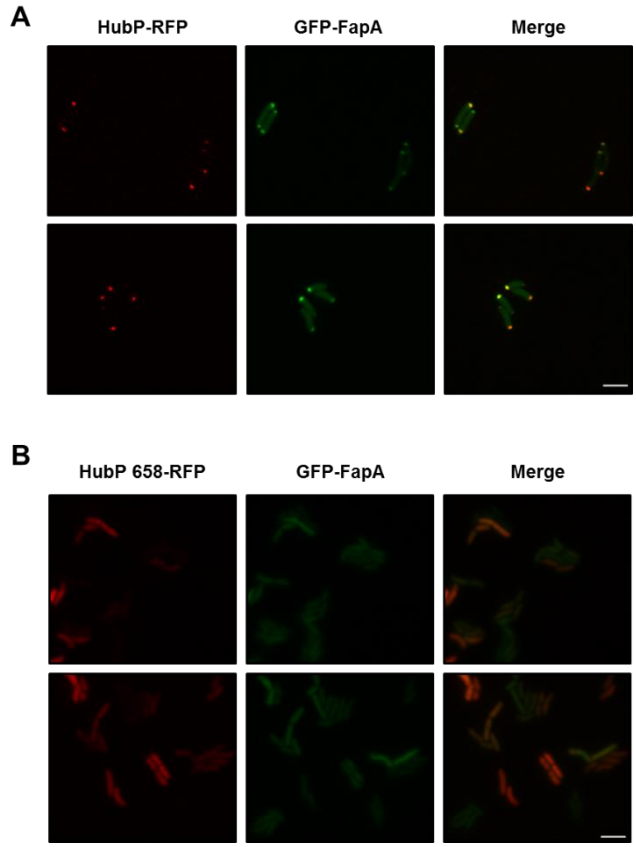

Figure 30. Co-localization of HubP-RFP and GFP-FapA.

HubP-RFP (A) or HubP 658-RFP (B) was expressed in Δ*hubP V. vulnificus* cells in the presence of GFP-FapA, and their subcellular localizations were monitored by fluorescence microscopy. Two representative fields are shown. Bars, 2 μm.

8.2. Sequestration of FapA from binding to HubP by dephosphorylated EIIA^{Glc}

Like *hubP* deletion strain, FapA mislocalization has been monitored in the wild-type strain when glucose was present (Figure 18A). At that time, FapA disappeared from the pole through direct interaction with dephosphorylated form of EIIA^{Glc} and flagellation was inhibited. This phenomenon led to explore correlation among EIIA^{Glc}, FapA, and HubP. It was speculated that EIIA^{Glc} could sequester FapA from HubP to inhibit polar targeting in the presence of glucose. To verify this assumption, the effect of EIIA^{Glc} on the HubP 658-FapA complex was examined by TALON metal affinity chromatography under various conditions (Figure 31). When PEP, EI, HPr were added to the reaction, EIIA^{Glc} was phosphorylated and could not disrupt the interaction between HubP 658 and His-FapA (lane 8 in Figure 31). When only EI and HPr were added to the reaction, however, dephosphorylated EIIA^{Glc} was combined and co-eluted with His-FapA (lane 7 in Figure 31). The band corresponding to the HubP 658 was also decreased compared with the mixture of HubP 658 and His-FapA (compare lanes 5 and 7 in Figure 31). Collectively, these results indicate that FapA can interact with only dephosphorylated form of the EIIA^{Glc} and then is sequestered from HubP.

9. Possible role of FapA in the early stage of flagellar assembly.

9.1. Effect of FapA mislocalization on flagella production in the *hubP* mutant

Previous observation of FapA mislocalization in the *hubP* mutant led to further explore the connection between HubP and flagellation of *V. vulnificus*. The *hubP* mutant exhibited motility defect in soft agar plates, similar to the *fapA* mutant (Figure 32B), and electron microscopy analyses

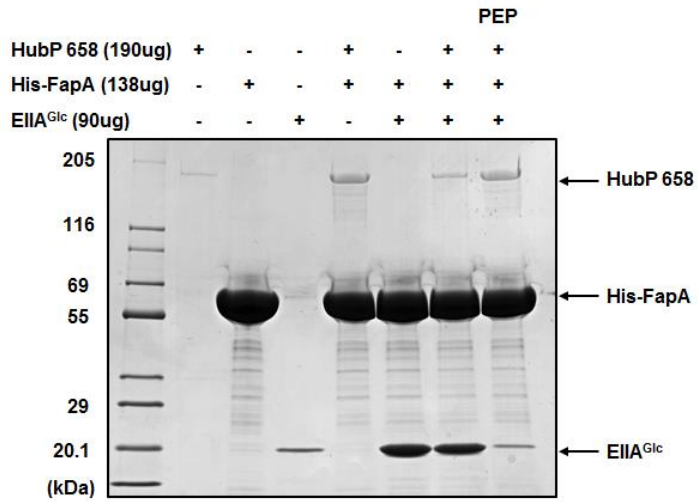

Figure 31. Effect of $EIIA^{Glc}$ on the formation of the HubP-FapA complex.

The effect of $EIIA^{Glc}$ on the HubP-FapA complex was examined by TALON metal affinity chromatography (Takara Bio) under various conditions. HubP 658 (190 μg), His-FapA (138 μg), and $EIIA^{Glc}$ (90 μg) were incubated at 37°C for 10 min in different combinations in 50 mM sodium phosphate buffer (pH 8.0) containing 2 mM $MgCl_2$, 200 mM KCl and 5 mM imidazole. Lane 1, EzWay Protein Blue MW Marker (KOMA BIOTECH); lane 2, HubP 658; lane 3, His-FapA; lane 4, $EIIA^{Glc}$; lane 5, HubP 658 and His-FapA; lane 6, $EIIA^{Glc}$ and His-FapA; lane 7, HubP 658, His-FapA, $EIIA^{Glc}$, EI and HPr; lane 8, HubP 658, His-FapA, $EIIA^{Glc}$, EI, HPr and PEP. Reaction mixtures were analyzed by SDS-PAGE using a 4-20% gradient gel (KOMA BIOTECH) and stained with Coomassie brilliant blue R.

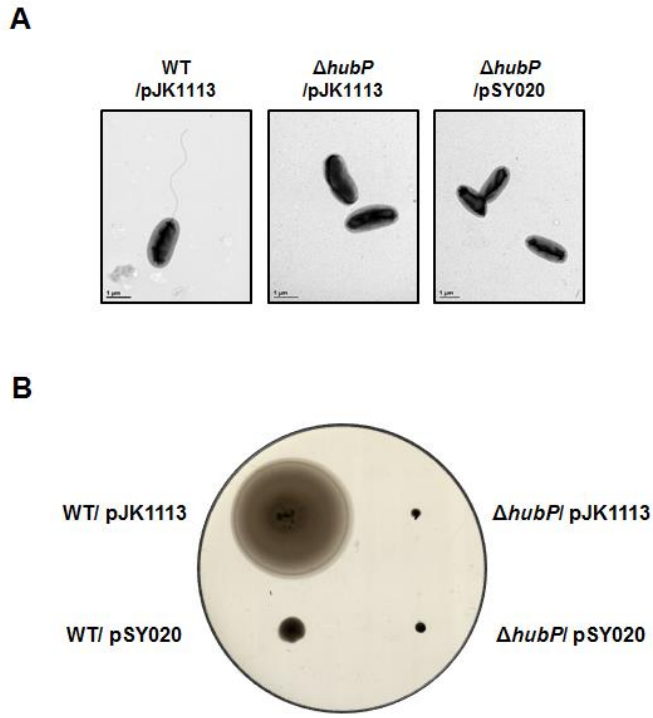

Figure 32. Swimming motility and flagella formation in indicated *V. vulnificus* strains.

A. Wild-type *V. vulnificus* cells harboring either the control vector pJK1113 and the *hubP* mutant cells harboring either pJK113 or pSY020 expressing wild-type HubP were grown to exponential phase in LBS medium supplemented with 0.002% (w/v) L-arabinose and negatively stained with 2% (w/v) uranyl acetate, and then observed using a transmission electron microscope. Bars, 1 μm.

B. Wild-type and *hubP* mutant strains harboring either pJK1113 or pSY020 were inoculated on a 0.3% agar LBS plate supplemented with 0.2% L-arabinose and incubated at 30°C for 16 h.

revealed that this loss of motility was turned out to be due to a complete failure of flagellation (Figure 32A). These results suggest that HubP induces flagellar assembly through a polar FapA-mediated mechanism. It is noteworthy that the motility and flagellation defect were not complemented in the *hubP* deletion strain by expression of the wild-type HubP in *trans* (Figure 32B). Moreover, the wild-type *V. vulnificus* strain harbouring the pJK1113-based HubP expression vector reduced motility. As previously shown, the right amount of polarly localized FapA is important for flagellar formation. Overexpressed HubP might interrupt FapA's sophisticated polar-targeting, and hence flagellation.

9.2. Effect of FapA on flagellar assembly

Several evidences suggest that HubP controls FapA's distribution and function for flagellar assembly via direct interactions. To verify the mechanism how polarly localized FapA helps flagellar assembly, the hook-basal bodies from wild-type, *fapA* mutant and *hubP* mutant strains were purified. Each fraction of purified hook-basal bodies was analyzed by SDS-PAGE and stained with Coomassie brilliant blue R (Figure 33A). Unexpectedly, the bands profile of the wild-type and the mutants were similar in the SDS-PAGE using a 4-20% gradient gel (KOMA BIOTECH). Because wild-type cell produces single flagellum and hook-basal body at only one pole, a large amount of the hook-basal body components might not have been obtained and hence perceived visually in the SDS-PAGE. To determine and compare purified hook-basal body components of the wild-type to those of the mutants, therefore, the bands profile of each strain were analyzed by mass spectrometry. Mass spectrometry analysis revealed that 26 of the hook-basal body components in 727 of total proteins were detected in the bands profile of the wild-type strain although only few hook-basal body components were detected in the *fapA* mutant and *hubP* mutant strains

(Table 4). It should be noted that similar basal bodies profile of two mutants provides strong evidence that FapA's polar targeting by HubP is important for flagellar assembly. The flagellar assembly is a orchestrated biochemical process involving both highly regulated flagellar gene expression and ordered protein assembly (Chevance et al. 2008; Minamino et al. 2015). Through the comparative analysis of detected hook-basal body components among wild-type, *fapA* mutant and *hubP* mutant strains, it was estimated that FapA seems to help assembly of export apparatus complex (Figure 33B and Table 4). However, the FapA-mediated specific mechanism remains to be determined.

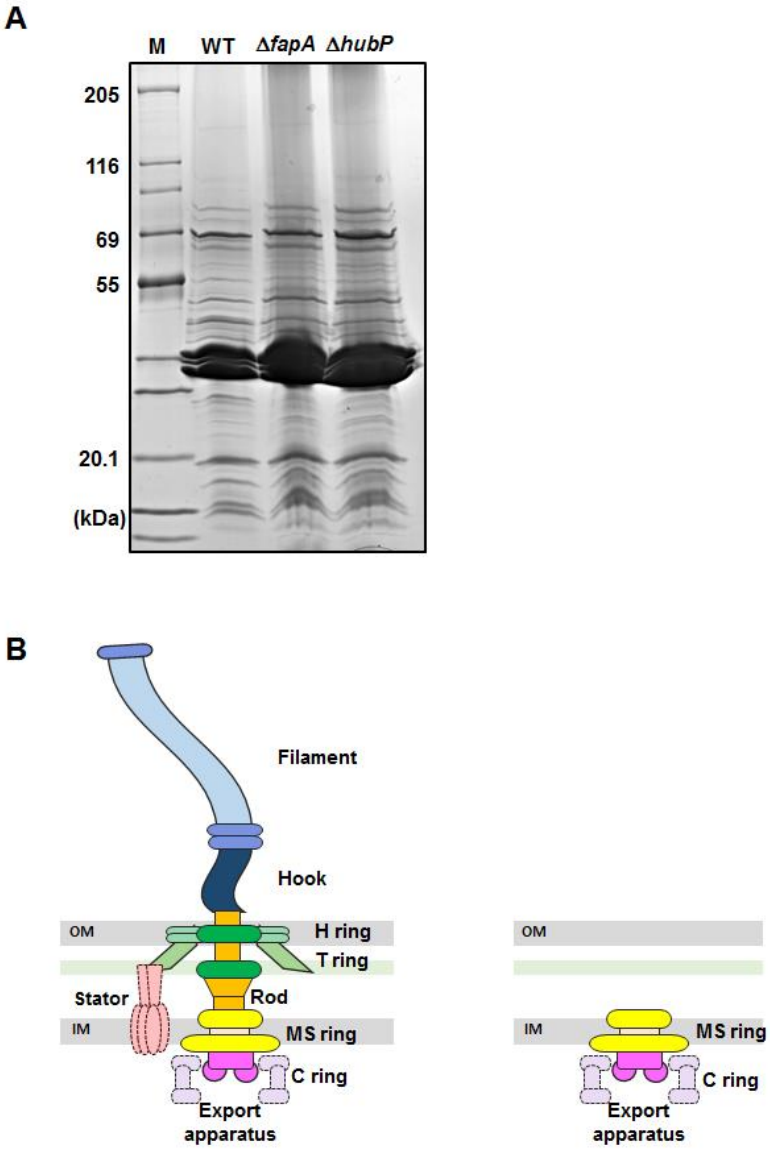
A
M
WT
ΔfapA
ΔhubP
205
116
69
55
20.1
(kDa)
B
Filament
Hook
OM
H ring
T ring
Stator
Rod
IM
MS ring
C ring
Export
apparatus
OM
IM
MS ring
C ring
Export
apparatus

Figure 33. Purification of the hook-basal bodies of *V. vulnificus*.

A. The proteins of the purified hook-basal body were analyzed by SDS-PAGE using a 4-20% gradient gel (KOMA BIOTECH) and stained with Coomassie brilliant blue R. M, EzWay Protein Blue MW Marker (KOMA BIOTECH).

B. Schematic presentation of expected flagellar basal bodies from wild-type (left) and mutant (right) strains. The components not detected by Mass spectrometry are marked in dotted lines.

Table 4. Detected proteins by mass spectrometry analysis

Description	Protein	Accession number	WT	Δ*fapA*	Δ*hubP*
Flagellar Structure					
MS ring	FliF	VVMO6_00818	O	-	-
Export apparatus	FliO	VVMO6_00827	O	O	O
	FliP	VVMO6_00828	O	-	-
Rod	FliE	VVMO6_00817	O	-	-
	FlgB	VVMO6_02266	O	-	-
	FlgC	VVMO6_02265	O	-	-
	FlgF	VVMO6_02262	O	-	-
	FlgG	VVMO6_02261	O	-	-
P ring	FlgI	VVMO6_02259	O	-	-
L ring	FlgH	VVMO6_02260	O	-	-
T ring	MotX	VVMO6_00247	O	-	-
	MotY	VVMO6_02035	O	-	-
H ring	FlgP	VVMO6_02272	O	-	-
	FlgT	VVMO6_02274	O	-	-
Hook	FlgE	VVMO6_02263	O	-	-
	FliK	VVMO6_00823	O	-	-
Hook-filament junction	FlgK	VVMO6_02257	O	-	-
	FlgL	VVMO6_02256	O	-	-
Flagellin	FlaF	VVMO6_00807	O	-	-
	FlaB/D	VVMO6_00808 VVMO6_02252	O	-*	-
	FlaA	VVMO6_00809	O	-	-
	FlaE	VVMO6_02251	O	-	-
	FlaC	VVMO6_02255	O	-	-
Filament cap	FliD	VVMO6_00811	O	-	-
House-keeping membrane protein					
Outer membrane protein	OmpU	VVMO6_00583	O	O	O
Outer membrane protein	OmpK	VVMO6_00699	O	O	O
Outer membrane protein	OmpT	VVMO6_00985	O	O	O
Outer membrane integrity protein	TolA	VVMO6_01035	O	O	O
Tol-Pal system periplasmic protein	TolB	VVMO6_01036	O	O	O

Outer membrane channel protein	TolC	VVMO6_04400	O	O	O
Potassium channel protein		VVMO6_01040	O	O	O
Sodium:proton antiporter		VVMO6_02494	O	O	O
Sodium:calcium antiporter		VVMO6_02682	O	O	O
PTS system, fructose-specific IIBC	FruA	VVMO6_03697	O	O	O
PTS system, ascorbate-specific IIC	UlaA	VVMO6_04230	O	O	O
Porin		VVMO6_01837	O	O	O
Chitoporin		VVMO6_02279	O	O	O
Glycerol MIP channel, aquaporin	GlpF	VVMO6_00679	O	O	O
Vitamin B12 transporter	BtuB	VVMO6_00146	O	O	O
Penicillin-binding protein 2	PBP2	VVMO6_02312	O	O	O
TonB-dependent heme receptor	HupA	VVMO6_03768	O	O	O
TonB-dependent siderophore receptor	VuuA	VVMO6_04211	O	O	O
Galactose ABC transporter substrate-binding protein	MglB	VVMO6_03135	O	O	O
ATP-dependent zinc metalloprotease	FtsH	VVMO6_00588	O	O	O
Multidrug ABC transporter permease		VVMO6_01651	O	O	O
Cytochrome C		VVMO6_00063	O	O	O

-*, represents detected, but negligible amount.

Chapter IV. Discussion

To compete successfully with others in a continually changing environment, an organism must prevent unnecessary consumption of energy and other resources by making a right decision to stay or move. Cells achieve molecular efficiency by using elegant control systems that monitor environmental changes and selectively decrease the synthesis of unnecessary proteins. One such system in bacteria is the PTS. The PTS enables bacteria to perceive and transport preferred carbon sources in the extracellular environment and control a variety of physiological processes depending on the availability and the nature of PTS sugars (Deutscher et al. 2006). In this study, it is found that *V. vulnificus* has developed a sophisticated mechanism for the PTS-dependent prevention of the unnecessary flagellar synthesis to stay in, but not move away from, glucose-rich niches. In the presence of glucose, the dephosphorylated form of $EIIA^{Glc}$ interacted with FapA, which turned out to be a critical factor regulating flagellar biosynthesis and motility. The FapA's polar localization by HubP was absolutely required for the flagellar assembly, and dephosphorylated $EIIA^{Glc}$ inhibited the polar localization of FapA through direct interaction (Figure 13 and 29).

While glucose is known as one of the most effective attractants, the flagellar biosynthesis has been known to be repressed in some bacteria when grown in a glucose-containing medium (Adler et al. 1967; Adler et al. 1973). Because glucose is the most preferred carbon source, bacteria use chemotactic motility to find a glucose-rich niche. Once they reach the glucose-rich environment, some bacteria seem to stop the flagellar biosynthesis to stay in this area until glucose is depleted. To date, this property has been reported only in glucose, but not in any other sugars and amino acids. Notably, although glucose-mediated inhibition of flagellar motility was also found in other proteobacteria, its molecular mechanism seems to be different between bacterial species. Unlike members of the

family *Enterobacteriaceae* such as *E. coli*, which use the cAMP-dependent mechanism (Yokota et al. 1970; Dobrogosz et al. 1971; Stella et al. 2008), *V. vulnificus* use the FapA-dependent mechanism to repress flagellation in the glucose-rich environment. Interestingly, while cAMP is known to be essential for flagellar motility in *E. coli* and many other species, the *cya* mutant of *V. vulnificus* retained the flagellar motility (Figure 8).

Flagellar synthesis and hence chemotactic motility has been extensively studied in the peritrichously flagellated bacteria *E. coli* (Armitage 1999; Stock et al. 2002). *E. coli* encodes four MCPs and single copies of each flagellar basal body and chemotaxis component. However, *Vibrio* species possess multiple paralogues of each component such as 6 copies of flagellin encoding genes and 45 MCP-like proteins, and several genes not found in *E.coli* such as *flhF*, *flhG*, and *cheY* (McCarter 2001). It is indicated that regulation of chemotactic signaling and motility in *Vibrio* species has additional complexity and multiplicity. Flagellar genes are hierarchically expressed under strict and intricate control in *Vibrio* and *Pseudomonas* species (Correa et al. 2005; Moisi et al. 2009). The only class I gene product, FlrA, activates class II genes that encode structural components and flagellar biosynthesis regulators such as FlhF, FlhG and FliA. The class II gene products regulate the expression of class III and IV genes encoding hook, additional basal body, and flagellins. While FlhF positively regulates the transcription of both class III and IV genes, FlhG negatively regulates the transcription of all four classes of flagellar promoters in the *Vibrionaceae* family (Correa et al. 2005). FapA shares several properties with FlhF. First, two genes are conserved in *Vibrio* species, but not found in *E. coli*. Second, deletion of either of the two genes results in a complete loss of flagellar assembly and motility (Figure 15) (Correa et al. 2005; Kusumoto et al. 2008; Kim et al. 2012). Third, the expression level of class III and class IV genes is decreased in both *fapA* and *flhF* mutants (Figure 17)

(Correa et al. 2005; Kim et al. 2012). Fourth, both proteins need to be localized at the flagellated pole for flagellar biosynthesis (Figure 16 and 18) (Kusumoto et al. 2008; Green et al. 2009). However, it is intriguing that the polar localization of the two proteins is independent of each other. A mutation in one gene did not influence the polar localization of the other gene product (Data not shown) because FapA is polar determined by direct interaction with HubP (Figure 23 and 29) while FlhF is polar targeted by HubP-independent mechanism (Yamaichi et al. 2012). Furthermore, while glucose delocalizes FapA from the flagellated pole, it did not affect the polar localization of FlhF (Figure 19). Another interesting difference between the two proteins is that, while flagellar synthesis and motility of a *V. vulnificus flhF* mutant could be restored to a wild-type level when FlhF was expressed from an arabinose-inducible plasmid in *trans* (Kim et al. 2012), the same phenotype of the *fapA* mutant could not be rescued by various FapA expression vectors tested in this study (Figure 20 and 21). Furthermore, uncontrolled expression of FapA resulted in a loss of flagellar motility even in the wild-type strain. Therefore, it is hypothesized that, unlike FlhF, FapA should be coordinately expressed with its upstream genes in the right amount in *V. vulnificus*. Interestingly, uncontrolled expression of HubP also resulted in a loss or reduction of flagellar motility (Figure 32), suggesting that the right amount of polarly targeted FapA through interaction with HubP is needed to flagellar assembly.

Connections between HubP and *vibrio* flagellation were previously reported (Yamaichi et al. 2012; Takekawa et al. 2016). Deletion of *hubP* appears to be involved in the inhibition of flagellar motility in *Vibrio* species. However, flagellation patterns were fairly inconsistent. Approximately 50% of *V. alginolyticus* cells formed multiple flagella in the absence of HubP. While deletion of *hubP* had a modest effect on flagellar number in *V. cholerae* of which 6% produced more than a single flagellum.

In *V. vulnificus*, *hubP* mutant was non-motile and this loss of motility was turned out to be due to a complete failure of flagellar assembly (Figure 32). In this study, it is determined that overall structure of HubP is conserved among HubP homologs (Figure 24). However, acidic repeats at cytoplasmic part of HubP homologs differ in length, copy number, and amino acid composition (Yamaichi et al. 2012; Rossmann et al. 2015; Takekawa et al. 2016). Because the cytoplasmic portions of HubP are required for interaction with its client proteins, different repeats might recruit different interaction partners and cause various effects on flagellation.

Purification of hook-basal bodies and mass spectrometry analysis revealed that the basal bodies profile of *hubP* deletion strain was similar to that of *fapA* deletion strain in *V. vulnificus* (Table 4). This result provides strong evidence that HubP-dependent recruitment of FapA to the *V. vulnificus* pole is crucial for flagella production. Furthermore, through mass spectrometry, it is expected that FapA affects the early stage of flagellar assembly. Because flagellar gene expression is controlled temporally and related tightly to assembly process (Chevance et al. 2008; Minamino et al. 2015), the decreased expression level of class III and class IV flagellar genes in *fapA* mutant (Figure 17) is relevant to result of the mass spectrometry analysis (Table 4). However, the biological rationale for the early stage of flagellar assembly by FapA remains to be determined.

To determine how HubP controls FapA-mediated flagellar synthesis at the cell poles and further interaction partners, protein ligand fishing experiment was performed (Data not shown). However, FapA, ParA and FlhG were not identified, although their interactions have been reported. It may suggest that the interactions between HubP and its clients are unstable, transient or dynamic. A polar land mark protein in α-proteobacterium *Caulobacter crescentus*, PopZ, is not homologous with HubP, but middle portion of PopZ is analogous to a cytoplasmic region of HubP (Holmes et al.

2016). It has been reported that the middle region of PopZ is intrinsically disordered, and its flexible structure shows various interfaces for interaction partners. Because cytoplasmic region of HubP might be intrinsically disorded and flexible, it is estimated that ligand fishing using HubP as baits was unsuccessful and FapA interacts randomly with the cytoplasmic part of HubP (Figure 27).

In summary, I have demonstrated that dephosphorylated $EIIA^{Glc}$ inhibits flagellation by sequestrating FapA from polar localized HubP in the presence of glucose and thereby enables cells to adapt to and stay in a glucose-rich environment (Figure 34). In future studies, it will be addressd the precise mechanism by which FapA controls the early stage of flagellar assembly.

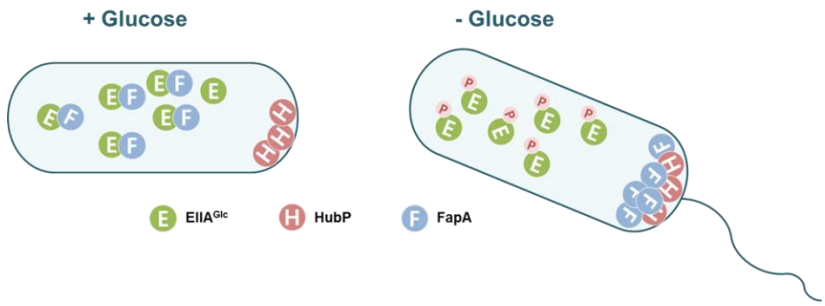

Figure 34. A model for the glucose-mediated inhibition of flagellar motility in *V. vulnificus*.

During the transport of glucose by the PTS, $EIIA^{Glc}$ is dephosphorylated and sequesters FapA from polar localized HubP by direct interaction. Delocalization of FapA causes inhibition of the flagellar assembly so that bacterial cells can stay in a glucose-rich environment until glucose is depleted. However, when glucose is depleted, FapA dissociates from phosphorylated $EIIA^{Glc}$ and free FapA can be localized back to the pole by direct interaction with HubP, where it triggers flagellation.

References

Adler J, Templeton B 1967. The effect of environmental conditions on the motility of *Escherichia coli*. J Gen Microbiol 46: 175-84.

Adler J, Hazelbauer GL, Dahl MM 1973. Chemotaxis toward sugars in *Escherichia coli*. J Bacteriol 115: 824-47.

Armitage JP 1999. Bacterial tactic responses. Adv Microb Physiol 41: 229-89.

Balaban M, Hendrixson DR 2011. Polar flagellar biosynthesis and a regulator of flagellar number influence spatial parameters of cell division in *Campylobacter jejuni*. PLoS Pathog 7: e1002420.

Balaban M, Joslin SN, Hendrixson DR 2009. FlhF and its GTPase activity are required for distinct processes in flagellar gene regulation and biosynthesis in *Campylobacter jejuni*. J Bacteriol 191: 6602-11.

Barabote RD, Saier MH, Jr. 2005. Comparative genomic analyses of the bacterial phosphotransferase system. Microbiol Mol Biol Rev 69: 608-34.

Boin MA, Austin MJ, Hase CC 2004. Chemotaxis in *Vibrio cholerae*. FEMS Microbiol Lett 239: 1-8.

Bren A, Eisenbach M 2001. Changing the direction of flagellar rotation in bacteria by modulating the ratio between the rotational states of the switch protein FliM. J Mol Biol 312: 699-709.

Butler SM, Camilli A 2005. Going against the grain: chemotaxis and infection in *Vibrio cholerae*. Nat Rev Microbiol 3: 611-20.

Chen X, Berg HC 2000. Solvent-isotope and pH effects on flagellar rotation in *Escherichia coli*. Biophys J 78: 2280-4.

Chevance FF, Hughes KT 2008. Coordinating assembly of a bacterial macromolecular machine. Nat Rev Microbiol 6: 455-65.

Chevance FF, Takahashi N, Karlinsey JEet al. 2007. The mechanism of outer membrane penetration by the eubacterial flagellum and implications for spirochete evolution. Genes Dev 21: 2326-35.

Chilcott GS, Hughes KT 2000. Coupling of flagellar gene expression to flagellar assembly in *Salmonella enterica* serovar typhimurium and *Escherichia coli*. Microbiol Mol Biol Rev 64: 694-708.

Chuang YC, Yuan CY, Liu CY, Lan CK, Huang AH 1992. *Vibrio vulnificus* infection in Taiwan: report of 28 cases and review of clinical manifestations and treatment. Clin Infect Dis 15: 271-6.

Colton DM, Stoudenmire JL, Stabb EV 2015. Growth on glucose decreases cAMP-CRP activity while paradoxically increasing intracellular cAMP in the light-organ symbiont *Vibrio fischeri*. Mol Microbiol 97: 1114-27.

Correa NE, Peng F, Klose KE 2005. Roles of the regulatory proteins FlhF and FlhG in the *Vibrio cholerae* flagellar transcription hierarchy. J Bacteriol 187: 6324-32.

Dalsgaard A, Frimodt-Moller N, Bruun B, Hoi L, Larsen JL 1996. Clinical manifestations and molecular epidemiology of *Vibrio vulnificus* infections in Denmark. Eur J Clin Microbiol Infect Dis 15: 227-32.

Deutscher J, Francke C, Postma PW 2006. How phosphotransferase system-related protein phosphorylation regulates carbohydrate metabolism in bacteria. Microbiol Mol Biol Rev 70: 939-1031.

Deutscher J, Ake FM, Derkaoui Met al. 2014. The bacterial phosphoenolpyruvate:carbohydrate phosphotransferase system: regulation by protein phosphorylation and phosphorylation-dependent protein-protein interactions. Microbiol Mol Biol Rev 78: 231-56.

Dobrogosz WJ, Hamilton PB 1971. The role of cyclic AMP in chemotaxis in *Escherichia coli*. Biochem Biophys Res Commun 42: 202-7.

Francis NR, Sosinsky GE, Thomas D, DeRosier DJ 1994. Isolation, characterization and structure of bacterial flagellar motors containing the switch complex. J Mol Biol 235: 1261-70.

Gardner AM, Gessner CR, Gardner PR 2003. Regulation of the nitric oxide reduction operon (norRVW) in *Escherichia coli*. Role of NorR and sigma54 in the nitric oxide stress response. J Biol Chem 278: 10081-6.

Gegner JA, Graham DR, Roth AF, Dahlquist FW 1992. Assembly of an MCP receptor, CheW, and kinase CheA complex in the bacterial chemotaxis signal transduction pathway. Cell 70: 975-82.

Gorke B, Stulke J 2008. Carbon catabolite repression in bacteria: many ways to make the most out of nutrients. Nat Rev Microbiol 6: 613-24.

Gray LD, Kreger AS 1987. Mouse skin damage caused by cytolysin from *Vibrio vulnificus* and by *V. vulnificus* infection. J Infect Dis 155: 236-41.

Green JC, Kahramanoglou C, Rahman A, Pender AM, Charbonnel N, Fraser GM 2009. Recruitment of the earliest component of the bacterial flagellum to the old cell division pole by a membrane-associated signal recognition particle family GTP-binding protein. J Mol Biol 391: 679-90.

Guan Y, Zhu Q, Huang D, Zhao S, Jan Lo L, Peng J 2015. An equation to estimate the difference between theoretically predicted and SDS PAGE-displayed molecular weights for an acidic peptide. Sci Rep 5: 13370.

Guttenplan SB, Shaw S, Kearns DB 2013. The cell biology of peritrichous flagella in *Bacillus subtilis*. Mol Microbiol 87: 211-29.

Heidelberg JF, Eisen JA, Nelson WCet al. 2000. DNA sequence of both chromosomes of the cholera pathogen *Vibrio cholerae*. Nature 406: 477-83.

Hirano T, Yamaguchi S, Oosawa K, Aizawa S 1994. Roles of FliK and FlhB in determination of flagellar hook length in *Salmonella typhimurium*. J Bacteriol 176: 5439-49.

Hiremath G, Hyakutake A, Yamamoto Ket al. 2015. Hypoxia-induced localization of chemotaxis-related signaling proteins in *Vibrio cholerae*. Mol Microbiol 95: 780-90.

Hlady WG, Klontz KC 1996. The epidemiology of Vibrio infections in Florida, 1981-1993. J Infect Dis 173: 1176-83.

Holmes JA, Follett SE, Wang H, Meadows CP, Varga K, Bowman GR 2016. *Caulobacter* PopZ forms an intrinsically disordered hub in organizing bacterial cell poles. Proc Natl Acad Sci U S A 113: 12490-12495.

Homma M, Iino T 1985. Locations of hook-associated proteins in flagellar structures of *Salmonella typhimurium*. J Bacteriol 162: 183-9.

Homma M, Kutsukake K, Hasebe M, Iino T, Macnab RM 1990. FlgB, FlgC, FlgF and FlgG. A family of structurally related proteins in the flagellar basal body of *Salmonella typhimurium*. J Mol Biol 211: 465-77.

Horseman MA, Surani S 2011. A comprehensive review of *Vibrio vulnificus*: an important cause of severe sepsis and skin and soft-tissue infection. Int J Infect Dis 15: e157-66.

Jeong HG, Satchell KJ 2012. Additive function of *Vibrio vulnificus* MARTX(Vv) and VvhA cytolysins promotes rapid growth and epithelial tissue necrosis during intestinal infection. PLoS Pathog 8: e1002581.

Jones MK, Oliver JD 2009. *Vibrio vulnificus*: disease and pathogenesis. Infect Immun 77: 1723-33.

Kazmierczak BI, Hendrixson DR 2013. Spatial and numerical regulation of flagellar biosynthesis in polarly flagellated bacteria. Mol Microbiol 88: 655-63.

Kearns DB 2010. A field guide to bacterial swarming motility. Nat Rev Microbiol 8: 634-44.

Keen NT, Tamaki S, Kobayashi D, Trollinger D 1988. Improved broad-host-range plasmids for DNA cloning in gram-negative bacteria. Gene 70: 191-7.

Kim HM, Park YH, Yoon CK, Seok YJ 2015. Histidine phosphocarrier protein regulates pyruvate kinase A activity in response to glucose in *Vibrio vulnificus*. Mol Microbiol 96: 293-305.

Kim HR, Rho HW, Jeong MHet al. 1993. Hemolytic mechanism of cytolysin produced from *V. vulnificus*. Life Sci 53: 571-7.

Kim SM, Lee DH, Choi SH 2012. Evidence that the *Vibrio vulnificus* flagellar regulator FlhF is regulated by a quorum sensing master regulator SmcR. Microbiology 158: 2017-25.

Kim YJ, Ryu Y, Koo BMet al. 2010. A mammalian insulysin homolog is regulated by enzyme IIA^{Glc} of the glucose transport system in *Vibrio vulnificus*. FEBS Lett 584: 4537-44.

Kim YK, McCarter LL 2000. Analysis of the polar flagellar gene system of *Vibrio parahaemolyticus*. J Bacteriol 182: 3693-704.

Kim YR, Haeng Rhee J 2003. Flagellar basal body flg operon as a virulence determinant of *Vibrio vulnificus*. Biochem Biophys Res Commun 304: 405-10.

Kim YR, Kim SY, Kim CM, Lee SE, Rhee JH 2005. Essential role of an adenylate cyclase in regulating *Vibrio vulnificus* virulence. FEMS Microbiol Lett 243: 497-503.

Kirkpatrick CL, Viollier PH 2011. Poles apart: prokaryotic polar organelles and their spatial regulation. Cold Spring Harb Perspect Biol 3.

Koo BM, Yoon MJ, Lee CRet al. 2004. A novel fermentation/respiration switch protein regulated by enzyme IIA^{Glc} in *Escherichia coli*. J Biol Chem 279: 31613-21.

Kundig W, Ghosh S, Roseman S 1964. Phosphate Bound to Histidine in a Protein as an Intermediate in a Novel Phospho-Transferase System.

Proc Natl Acad Sci U S A 52: 1067-74.

Kusumoto A, Shinohara A, Terashima H, Kojima S, Yakushi T, Homma M 2008. Collaboration of FlhF and FlhG to regulate polar-flagella number and localization in *Vibrio alginolyticus*. Microbiology 154: 1390-9.

Lawley B, Sims IM, Tannock GW 2013. Whole-transcriptome shotgun sequencing (RNA-seq) screen reveals upregulation of cellobiose and motility operons of *Lactobacillus ruminis* L5 during growth on tetrasaccharides derived from barley beta-glucan. Appl Environ Microbiol 79: 5661-9.

Lee BC, Kim SH, Choi SH, Kim TS 2005. Induction of interleukin-8 production via nuclear factor-kappaB activation in human intestinal epithelial cells infected with *Vibrio vulnificus*. Immunology 115: 506-15.

Lee CR, Cho SH, Yoon MJ, Peterkofsky A, Seok YJ 2007. *Escherichia coli* enzyme IIA^{Ntr} regulates the K^+ transporter TrkA. Proc Natl Acad Sci U S A 104: 4124-9.

Lee CR, Kim M, Park YH, Kim YR, Seok YJ 2014. RppH-dependent pyrophosphohydrolysis of mRNAs is regulated by direct interaction with DapF in *Escherichia coli*. Nucleic Acids Res 42: 12746-57.

Lee JH, Rho JB, Park KJet al. 2004. Role of flagellum and motility in pathogenesis of *Vibrio vulnificus*. Infect Immun 72: 4905-10.

Lee KJ, Jeong CS, An YJet al. 2011. FrsA functions as a cofactor-independent decarboxylase to control metabolic flux. Nat Chem Biol 7: 434-6.

Leng Y, Vakulskas CA, Zere TRet al. 2016. Regulation of CsrB/C sRNA decay by $EIIA^{Glc}$ of the phosphoenolpyruvate: carbohydrate phosphotransferase system. Mol Microbiol 99: 627-39.

Levy S, Zeng GQ, Danchin A 1990. Cyclic AMP synthesis in *Escherichia*

coli strains bearing known deletions in the pts phosphotransferase operon. Gene 86: 27-33.

Lim JG, Bang YJ, Choi SH 2014. Characterization of the *Vibrio vulnificus* 1-Cys peroxiredoxin Prx3 and regulation of its expression by the Fe-S cluster regulator IscR in response to oxidative stress and iron starvation. J. Biol. Chem. 289: 36263-74.

Linkous DA, Oliver JD 1999. Pathogenesis of *Vibrio vulnificus*. FEMS Microbiol Lett 174: 207-14.

Magariyama Y, Sugiyama S, Muramoto Ket al. 1994. Very fast flagellar rotation. Nature 371: 752.

Mauriello EM, Mignot T, Yang Z, Zusman DR 2010. Gliding motility revisited: how do the myxobacteria move without flagella? Microbiol Mol Biol Rev 74: 229-49.

McCarter LL 2001. Polar flagellar motility of the *Vibrionaceae*. Microbiol Mol Biol Rev 65: 445-62, table of contents.

McPherson VL, Watts JA, Simpson LM, Oliver JD 1991. Physiological effects of the lipopolysaccharide of *Vibrio vulnificus* on mice and rats. Microbios 67: 141-9.

Merkel SM, Alexander S, Zufall E, Oliver JD, Huet-Hudson YM 2001. Essential role for estrogen in protection against *Vibrio vulnificus*-induced endotoxic shock. Infect Immun 69: 6119-22.

Miller VL, Mekalanos JJ 1988. A novel suicide vector and its use in construction of insertion mutations: osmoregulation of outer membrane proteins and virulence determinants in *Vibrio cholerae* requires toxR. J. Bacteriol. 170: 2575-83.

Milton DL, O'Toole R, Horstedt P, Wolf-Watz H 1996. Flagellin A is essential for the virulence of *Vibrio anguillarum*. J. Bacteriol. 178: 1310-9.

Minamino T, Imada K 2015. The bacterial flagellar motor and its structural

diversity. Trends Microbiol 23: 267-74.

Moisi M, Jenul C, Butler SMet al. 2009. A novel regulatory protein involved in motility of *Vibrio cholerae*. J Bacteriol 191: 7027-38.

Nam TW, Park YH, Jeong HJ, Ryu S, Seok YJ 2005. Glucose repression of the *Escherichia coli* sdhCDAB operon, revisited: regulation by the CRP*cAMP complex. Nucleic Acids Res 33: 6712-22.

Nam TW, Cho SH, Shin Det al. 2001. The *Escherichia coli* glucose transporter enzyme $IICB^{Glc}$ recruits the global repressor Mlc. EMBO J 20: 491-8.

Ottemann KM, Miller JF 1997. Roles for motility in bacterial-host interactions. Mol Microbiol 24: 1109-17.

Park JH, Cho YJ, Chun Jet al. 2011. Complete genome sequence of *Vibrio vulnificus* MO6-24/O. J Bacteriol 193: 2062-3.

Park KH, Kim JS, Lee YRet al. 2007. Low-density lipoprotein protects *Vibrio vulnificus*-induced lethality through blocking lipo-polysaccharide action. Exp Mol Med 39: 673-8.

Park YH, Lee BR, Seok YJ, Peterkofsky A 2006. In vitro reconstitution of catabolite repression in *Escherichia coli*. J Biol Chem 281: 6448-54.

Park YH, Lee CR, Choe M, Seok YJ 2013. HPr antagonizes the anti-sigma70 activity of Rsd in *Escherichia coli*. Proc Natl Acad Sci U S A 110: 21142-7.

Peterkofsky A, Reizer A, Reizer J, Gollop N, Zhu PP, Amin N 1993. Bacterial adenylyl cyclases. Prog Nucleic Acid Res Mol Biol 44: 31-65.

Phillips KE, Satchell KJ 2017. *Vibrio vulnificus*: From Oyster Colonist to Human Pathogen. PLoS Pathog 13: e1006053.

Postma PW, Lengeler JW, Jacobson GR 1993. Phosphoenolpyruvate: carbohydrate phosphotransferase systems of bacteria. Microbiol Rev 57: 543-94.

Ringgaard S, Hubbard T, Mandlik A, Davis BM, Waldor MK 2015. RpoS and quorum sensing control expression and polar localization of *Vibrio cholerae* chemotaxis cluster III proteins *in vitro* and *in vivo*. Mol Microbiol 97: 660-75.

Ringgaard S, Zepeda-Rivera M, Wu X, Schirner K, Davis BM, Waldor MK 2014. ParP prevents dissociation of CheA from chemotactic signaling arrays and tethers them to a polar anchor. Proc Natl Acad Sci U S A 111: E255-64.

Rossmann F, Brenzinger S, Knauer Cet al. 2015. The role of FlhF and HubP as polar landmark proteins in *Shewanella putrefaciens* CN-32. Mol Microbiol 98: 727-42.

Roy A, Danchin A, Joseph E, Ullmann A 1983. Two functional domains in adenylate cyclase of *Escherichia coli*. J Mol Biol 165: 197-202.

Schuhmacher JS, Thormann KM, Bange G 2015. How bacteria maintain location and number of flagella? FEMS Microbiol Rev 39: 812-22.

Schuster SC, Swanson RV, Alex LA, Bourret RB, Simon MI 1993. Assembly and function of a quaternary signal transduction complex monitored by surface plasmon resonance. Nature 365: 343-7.

Semmler AB, Whitchurch CB, Leech AJ, Mattick JS 2000. Identification of a novel gene, fimV, involved in twitching motility in *Pseudomonas aeruginosa*. Microbiology 146 (Pt 6): 1321-32.

Siebold C, Flukiger K, Beutler R, Erni B 2001. Carbohydrate transporters of the bacterial phosphoenolpyruvate: sugar phosphotransferase system (PTS). FEBS Lett 504: 104-11.

Smith AB, Siebeling RJ 2003. Identification of genetic loci required for capsular expression in *Vibrio vulnificus*. Infect Immun 71: 1091-7.

Springer WR, Koshland DE, Jr. 1977. Identification of a protein methyltransferase as the cheR gene product in the bacterial sensing system. Proc Natl Acad Sci U S A 74: 533-7.

Stella NA, Kalivoda EJ, O'Dee DM, Nau GJ, Shanks RM 2008. Catabolite repression control of flagellum production by *Serratia marcescens*. Res Microbiol 159: 562-8.

Stock JB, Levit MN, Wolanin PM 2002. Information processing in bacterial chemotaxis. Sci STKE 2002: pe25.

Strom MS, Paranjpye RN 2000. Epidemiology and pathogenesis of *Vibrio vulnificus*. Microbes Infect 2: 177-88.

Takekawa N, Kwon S, Nishioka N, Kojima S, Homma M 2016. HubP, a Polar Landmark Protein, Regulates Flagellar Number by Assisting in the Proper Polar Localization of FlhG in *Vibrio alginolyticus*. J Bacteriol 198: 3091-3098.

Tal M, Silberstein A, Nusser E 1985. Why does Coomassie Brilliant Blue R interact differently with different proteins? A partial answer. J Biol Chem 260: 9976-80.

Terashima H, Fukuoka H, Yakushi T, Kojima S, Homma M 2006. The *Vibrio* motor proteins, MotX and MotY, are associated with the basal body of Na-driven flagella and required for stator formation. Mol Microbiol 62: 1170-80.

Terashima H, Li N, Sakuma Met al. 2013. Insight into the assembly mechanism in the supramolecular rings of the sodium-driven *Vibrio* flagellar motor from the structure of FlgT. Proc Natl Acad Sci U S A 110: 6133-8.

Ueno T, Oosawa K, Aizawa S 1992. M ring, S ring and proximal rod of the flagellar basal body of *Salmonella typhimurium* are composed of subunits of a single protein, FliF. J Mol Biol 227: 672-7.

van Amsterdam K, van der Ende A 2004. *Helicobacter pylori* HP1034 (*ylxH*) is required for motility. Helicobacter 9: 387-95.

Wehbi H, Portillo E, Harvey Het al. 2011. The peptidoglycan-binding protein FimV promotes assembly of the *Pseudomonas aeruginosa*

type IV pilus secretin. J Bacteriol 193: 540-50.

Wilson CM 1979. Studies and critique of Amido Black 10B, Coomassie Blue R, and Fast Green FCF as stains for proteins after polyacrylamide gel electrophoresis. Anal Biochem 96: 263-78.

Wright AC, Morris JG, Jr. 1991. The extracellular cytolysin of *Vibrio vulnificus*: inactivation and relationship to virulence in mice. Infect Immun 59: 192-7.

Wright AC, Simpson LM, Oliver JD, Morris JG, Jr. 1990. Phenotypic evaluation of acapsular transposon mutants of *Vibrio vulnificus*. Infect. Immun. 58: 1769-73.

Wright AC, Powell JL, Tanner MKet al. 1999. Differential expression of *Vibrio vulnificus* capsular polysaccharide. Infect Immun 67: 2250-7.

Xie L, Altindal T, Chattopadhyay S, Wu XL 2011. From the Cover: Bacterial flagellum as a propeller and as a rudder for efficient chemotaxis. Proc Natl Acad Sci U S A 108: 2246-51.

Yamaichi Y, Bruckner R, Ringgaard Set al. 2012. A multidomain hub anchors the chromosome segregation and chemotactic machinery to the bacterial pole. Genes Dev 26: 2348-60.

Yokota T, Gots JS 1970. Requirement of adenosine 3', 5'-cyclic phosphate for flagella formation in *Escherichia coli* and *Salmonella typhimurium*. J Bacteriol 103: 513-6.

Yonekawa H, Hayashi H, Parkinson JS 1983. Requirement of the cheB function for sensory adaptation in *Escherichia coli*. J Bacteriol 156: 1228-35.

Yonekura K, Maki S, Morgan DGet al. 2000. The bacterial flagellar cap as the rotary promoter of flagellin self-assembly. Science 290: 2148-52.

Zhu S, Kojima S, Homma M 2013. Structure, gene regulation and environmental response of flagella in *Vibrio*. Front Microbiol 4: 410.

Zhu S, Nishikino T, Hu B, Kojima S, Homma M, Liu J 2017. Molecular

architecture of the sheathed polar flagellum in *Vibrio alginolyticus*. Proc Natl Acad Sci U S A 114: 10966-10971.

국문 초록

세균은 변화하는 환경에 잘 적응하기 위해 유인물질 또는 기피물질의 농도 구배를 감지하고, 더 유익한 서식지가 나올 때까지 의도적으로 이동한다. 포도당은 가장 효과적인 유인물질이지만, 일부 세균에서는 편모합성 및 운동성을 억제한다고 알려져 있다. 현재까지, 일부 주모균에서 이차신호전달물질인 cAMP의 양을 하향조절함으로써 포도당에 의한 편모합성을 저해한다고 알려져 있었지만, 정확한 기작은 밝혀져 있지 않았다. 따라서 본 연구를 통하여, 단모균인 패혈증 비브리오균에서도 포도당 관련 편모합성 저해가 관찰되는지, 그리고 그 기작은 무엇인지 밝히고자 하였다.

패혈증 비브리오균은 다른 세균과 마찬가지로 포도당에 의해 편모합성 및 운동성이 억제되지만, 다른 기작을 통하여 조절되는 것으로 확인되었다. 포도당이 있는 조건에서, 세균의 포도당 특이적인 PTS (phosphoenolpyruvate: sugar phosphotransferase system)의 구성 단백질인 Enzyme IIA^{Glc} ($EIIA^{Glc}$)는 탈 인산화되고, 탈 인산화된 $EIIA^{Glc}$는 FapA (Flagellar assembly protein A)와 상호작용한다. 이들의 결합은 편모가 존재하는 pole에 위치한 FapA의 비편재화를 유도하여 편모 합성 및 운동성을 억제한다. 그러나 포도당이 고갈되면, $EIIA^{Glc}$는 인산화되어 FapA와 결합하지 못하고, 이때 FapA는 다시 pole로 이동하여 편모합성을 유도하는 것으로 확인되었다.

FapA가 어떻게 pole로 이동하고 편모합성에 영향을 미치는지 세부적인 기작을 알아내기 위하여, ligand fishing 실험을 수행하였다. 그 결과 FapA가 $EIIA^{Glc}$ 뿐만 아니라 HubP (Hub of the pole)와 상호작용한다는 것을 알 수 있었다. HubP는 pole의 랜드마크

단백질로 염색체 분리, 주화성 구성요소 및 편모합성에 관여하는 단백질들과 상호작용하여 pole로 이동시킨 후 이들의 기능을 조절한다. HubP의 결손이 FapA의 비 편재화를 유도하는 것을 관찰함으로써, HubP는 FapA가 pole로 이동하는 결정요인이라는 것을 확인했다.

이러한 결과들로부터, 패혈증 비브리오균이 포도당이 풍부한 환경에 도달하고 머무르는 새로운 전략을 파악할 수 있었다. 포도당이 고갈되면, $EIIA^{Glc}$는 인산화 되고, FapA는 HubP와 결합하여 pole로 이동하여 편모합성을 유도함으로써 세균의 이동을 돕는다. 반면에, 포도당이 풍부한 환경에서는 탈 인산화 된 $EIIA^{Glc}$ 가 FapA와 상호작용하여 pole에 위치한 FapA를 비 편재화시킨다. 이를 통해 FapA의 기능을 억제함으로써 세균이 머무를 수 있도록 유도한다.

주요어:
패혈증 비브리오균, 편모합성, PTS, Enzyme IIA^{Glc}, FapA, HubP

학번: 2012-31269